NASA TECHNICAL MEMORANDUM

NASA TM X-2413

NASA TM X-2413

FLIGHT-DETERMINED AERODYNAMIC STABILITY AND CONTROL DERIVATIVES OF THE M2-F2 LIFTING BODY VEHICLE AT SUBSONIC SPEEDS

by Robert W. Kempel and Ronald C. Thompson

Flight Research Center
Edwards, Calif. 93523

NATIONAL AERONAUTICS AND SPACE ADMINISTRATION • WASHINGTON, D. C. • DECEMBER 1971

1. Report No.	2. Government Accession No.	3. Recipient's Catalog No.
NASA TM X-2413		

4. Title and Subtitle	5. Report Date
FLIGHT-DETERMINED AERODYNAMIC STABILITY AND CONTROL DERIVATIVES OF THE M2-F2 LIFTING BODY VEHICLE AT SUBSONIC SPEEDS	December 1971
	6. Performing Organization Code

7. Author(s)	8. Performing Organization Report No.
Robert W. Kempel and Ronald C. Thompson	H-520
	10. Work Unit No.
	727-00-00-01-24

9. Performing Organization Name and Address	11. Contract or Grant No.
NASA Flight Research Center P. O. Box 273 Edwards, California 93523	
	13. Type of Report and Period Covered
	Technical Memorandum

12. Sponsoring Agency Name and Address	14. Sponsoring Agency Code
National Aeronautics and Space Administration Washington, D. C. 20546	

15. Supplementary Notes

16. Abstract

Aerodynamic derivatives were obtained for the M2-F2 lifting body flight vehicle in the subsonic flight region between Mach numbers of 0.41 and 0.64 and altitudes of 2130 meters (7000 feet) to 13,730 meters (45,000 feet). The derivatives were determined by a flight time history curve-fitting process utilizing a hybrid computer. The flight-determined derivatives are compared with wind-tunnel and predicted values. Modal-response characteristics, calculated from the flight derivatives, are presented.

17. Key Words (Suggested by Author(s))	18. Distribution Statement
Aerodynamic stability derivatives M2-F2 lifting body flight vehicle	Unclassified - Unlimited

19. Security Classif. (of this report)	20. Security Classif. (of this page)	21. No. of Pages	22. Price*
Unclassified	Unclassified	33	$3.00

*For sale by the National Technical Information Service, Springfield, Virginia 22151

FLIGHT-DETERMINED AERODYNAMIC STABILITY AND CONTROL DERIVATIVES OF THE M2-F2 LIFTING BODY VEHICLE AT SUBSONIC SPEEDS

Robert W. Kempel and Ronald C. Thompson
Flight Research Center

SUMMARY

The longitudinal and lateral-directional stability and control derivatives determined from flight tests of the M2-F2 lifting body research vehicle are presented for a range of Mach numbers from 0.41 to 0.64 and for angles of attack from -2.3° to 13.8°. The derivatives were determined by using a high-speed repetitive analog-matching technique and approximate equations to analyze recorded time histories of vehicle response to random control inputs and pulses. The flight-determined derivatives were compared with wind-tunnel predictions for representative Mach number and angle-of-attack conditions. Using these derivatives, the vehicle modal-response characteristics were calculated.

Comparisons of flight and wind-tunnel results indicated that the flight-determined longitudinal aerodynamic static stability, lower-flap effectiveness, and pitch damping were generally higher than predicted. The normal-force-curve slope as well as the lateral-directional aerodynamic stability and control effectiveness generally agreed with wind-tunnel predictions. In general, the lateral-directional-damping derivatives were in good agreement with predictions.

INTRODUCTION

The first manned flight tests of lifting body reentry vehicle configurations were made at the NASA Flight Research Center, Edwards, Calif., under the joint sponsorship of NASA and the U. S. Air Force. The test program was designed to investigate performance, stability and control, and flying-quality requirements of this new class of vehicle throughout the subsonic, transonic, and low supersonic flight regions. Testing was started with the lightweight M2-F1 vehicle; the results of these tests are reported in reference 1. Subsequently, to expand the limited performance envelope of the basic M2-F1, a heavier and more sophisticated vehicle, the M2-F2, was designed and built. The M2-F2 was designed for launch from a B-52 carrier aircraft and was capable of either a glide flight to landing or an accelerated flight to higher altitudes and speeds utilizing a modified LR-11 rocket engine, followed by a glide flight to landing. The first glide flight of the M2-F2 was made on July 12, 1966; in the following 8 months, 16 glide flights were completed. On the last flight, before the powered phase of the program, the vehicle was damaged extensively in a gear-up landing.

Even though the powered phase of the program was not conducted, the initial glide

tests served many important functions. Prior to the flight program, predictions of the flight characteristics of lifting bodies were, by necessity, based almost exclusively on wind-tunnel data. The flight program did, therefore, make it possible to compare the extensive small-scale and limited full-scale wind-tunnel results with the actual flight data in order to establish some measure of prediction accuracy. In addition, a hybrid computer program was mechanized for the determination of flight derivatives based on a curve-fitting technique which used the data obtained from the flight program. The flight results also made possible an assessment of the sensitivity of handling qualities to typical discrepancies between predicted and actual flight derivative values.

In this report the more significant longitudinal and lateral-directional aerodynamic stability and control derivatives obtained from flight are compared with small- and full-scale wind-tunnel results. The modal-response characteristics calculated from the flight-determined derivatives are included.

General stability and control flight results for the M2-F2 vehicle are reported in reference 2, and performance, lift, and drag results are reported in reference 3.

SYMBOLS

Data are presented as standard NASA coefficients of forces and moments which are referred to the vehicle body axes fixed with respect to the vehicle center of gravity. Positive directions are: X, forward; Y, to the right; and Z, down. Positive directions of the forces, moments, and angular displacements and velocities are in accord with the right-hand rule.

Physical quantities are given in the International System of Units (SI) and parenthetically in U. S. Customary Units. The measurements were taken in U. S. Customary Units. Factors relating the two systems are presented in reference 4.

a_n normal acceleration, g

a_y transverse acceleration, g

b reference body span, m (ft)

C_l rolling-moment coefficient, $\frac{\text{Rolling moment}}{\bar{q}Sb}$

C_{l_p} roll-damping derivative, $\frac{\partial C_l}{\partial \frac{pb}{2V}}$, per rad

C_{l_r} change in rolling-moment coefficient with yaw rate, $\frac{\partial C_l}{\partial \frac{rb}{2V}}$, per rad

C_{l_β} effective-dihedral derivative, $\frac{\partial C_l}{\partial \beta}$, per deg

$C_{l_{\delta_a}}$ aileron-effectiveness derivative, $\frac{\partial C_l}{\partial \delta_a}$, per deg

$C_{l_{\delta_r}}$ change in rolling-moment coefficient with rudder deflection, $\frac{\partial C_l}{\partial \delta_r}$, per deg

C_m pitching-moment coefficient, $\frac{\text{Pitching moment}}{\bar{q}S\bar{c}}$

C_{m_q} pitch-damping derivative, $\frac{\partial C_m}{\partial \frac{q\bar{c}}{2V}}$, per rad

C_{m_α} static longitudinal-stability derivative, $\frac{\partial C_m}{\partial \alpha}$, per deg

$C_{m_{\delta_l}}$ lower-flap-effectiveness derivative, $\frac{\partial C_m}{\partial \delta_l}$, per deg

C_N normal-force coefficient, $\frac{\text{Normal force}}{\bar{q}S}$

C_{N_α} normal-force-curve slope, $\frac{\partial C_N}{\partial \alpha}$, per deg

$C_{N_{\delta_l}}$ change in normal-force coefficient with lower-flap deflection, $\frac{\partial C_N}{\partial \delta_l}$, per deg

C_n yawing-moment coefficient, $\frac{\text{Yawing moment}}{\bar{q}Sb}$

C_{n_p} change in yawing-moment coefficient with roll rate, $\frac{\partial C_n}{\partial \frac{pb}{2V}}$, per rad

C_{n_r} yaw-damping derivative, $\frac{\partial C_n}{\partial \frac{rb}{2V}}$, per rad

C_{n_β} directional-stability derivative, $\frac{\partial C_n}{\partial \beta}$, per deg

$C_{n_{\delta_a}}$ change in yawing-moment coefficient with aileron deflection, $\frac{\partial C_n}{\partial \delta_a}$, per deg

$C_{n_{\delta_r}}$ rudder-effectiveness derivative, $\frac{\partial C_n}{\partial \delta_r}$, per deg

C_Y side-force coefficient, $\frac{\text{Side force}}{\bar{q}S}$

C_{Y_β} side-force derivative, $\frac{\partial C_Y}{\partial \beta}$, per deg

$C_{Y_{\delta_a}}$ change in side-force coefficient with aileron deflection, $\frac{\partial C_Y}{\partial \delta_a}$, per deg

$C_{Y_{\delta_r}}$ change in side-force coefficient with rudder deflection, $\frac{\partial C_Y}{\partial \delta_r}$, per deg

$\bar{c}$ reference longitudinal length, m (ft)

g acceleration due to gravity, 9.80 m/sec^2 (32.2 ft/sec^2)

h_p pressure altitude, m (ft)

I_X rolling moment of inertia, kg-m^2 (slug-ft^2)

I_{XZ} product of inertia, kg-m^2 (slug-ft^2)

I_Y pitching moment of inertia, kg-m^2 (slug-ft^2)

I_Z yawing moment of inertia, kg-m^2 (slug-ft^2)

L_p dimensionalized roll-damping derivative, $\frac{\bar{q}Sb^2}{2VI_X}C_{l_p}$, per sec

L_r dimensionalized rolling moment due to yaw rate, $\frac{\bar{q}Sb^2}{2VI_X}C_{l_r}$, per sec

L_β dimensionalized effective-dihedral derivative, $\frac{\bar{q}Sb}{I_X}C_{l_\beta}$, per sec^2

L_{δ_a} dimensionalized aileron-effectiveness derivative, $\frac{\bar{q}Sb}{I_X}C_{l_{\delta_a}}$, per sec^2

L_{δ_r} — dimensionalized rolling moment due to rudder deflection, $\frac{\bar{q}Sb}{I_X} C_{l_{\delta_r}}$, per sec^2

M — Mach number

M_q — dimensionalized pitch-damping derivative, $\frac{\bar{q}S\bar{c}^2}{2VI_Y} C_{m_q}$, per sec

M_w — dimensionalized longitudinal-stability derivative, $\frac{\bar{q}S\bar{c}}{VI_Y} C_{m_\alpha}$, per sec

M_{δ_l} — dimensionalized lower-flap-effectiveness derivative, $\frac{\bar{q}S\bar{c}}{I_Y} C_{m_{\delta_l}}$, per sec^2

m — mass, kg (slugs)

N_p — dimensionalized yawing moment due to roll rate, $\frac{\bar{q}Sb^2}{2VI_Z} C_{n_p}$, per sec

N_r — dimensionalized yaw-damping derivative, $\frac{\bar{q}Sb^2}{2VI_Z} C_{n_r}$, per sec

N_β — dimensionalized directional-stability derivative, $\frac{\bar{q}Sb}{I_Z} C_{n_\beta}$, per sec^2

N_{δ_a} — dimensionalized yawing moment due to aileron deflection, $\frac{\bar{q}Sb}{I_Z} C_{n_{\delta_a}}$, per sec^2

N_{δ_r} — dimensionalized rudder-effectiveness derivative, $\frac{\bar{q}Sb}{I_Z} C_{n_{\delta_r}}$, per sec^2

P — period of transient oscillation, sec

p, q, r — rolling, pitching, and yawing angular rate, respectively, deg/sec

$\bar{q}$	dynamic pressure, $\frac{1}{2}\rho V^2$, N/m^2 (lb/ft^2)
S	reference planform area, m^2 (ft^2)
$T_{1/2}$	time required for transient response to damp to half amplitude, $\frac{0.693}{\zeta \omega_n}$, sec
t	time, sec
V	true airspeed, m/sec (ft/sec)
W	vehicle weight, kg (lb)
w	linear perturbed velocity along vehicle Z-axis, m/sec (ft/sec)
X, Y, Z	reference coordinates, cm (in.)
Y_β	dimensionalized side-force derivative, $\frac{\bar{q}S}{mV} C_{Y_\beta}$, per sec
Y_{δ_a}	dimensionalized side force due to aileron deflection, $\frac{\bar{q}S}{mV} C_{Y_{\delta_a}}$, per sec
Y_{δ_r}	dimensionalized side force due to rudder deflection, $\frac{\bar{q}S}{mV} C_{Y_{\delta_r}}$, per sec
Z_w	dimensionalized variation of normal force with w, $\frac{\bar{q}S}{mV}\left(-C_{N_\alpha}\right)$, per sec
Z_{δ_l}	dimensionalized variation of normal force with δ_l, $\frac{\bar{q}S}{mV}\left(-C_{N_{\delta_l}}\right)$, m/sec^2 (ft/sec^2)
α	angle of attack, deg
β	angle of sideslip, deg
Δ	incremental value

δ_a	aileron deflection, $\left(\delta_{u_L} - \delta_{u_R}\right)$, deg
δ_l	lower-flap deflection, deg
δ_r	rudder deflection, $\delta_{r_L} - \left\|\delta_{r_R}\right\|$, deg
δ_u	average upper-flap position, $\frac{1}{2}\left(\delta_{u_L} + \delta_{u_R}\right)$, deg
ϵ	inclination of principal axis, deg
ζ	damping ratio
Θ	pitch attitude, deg
ρ	atmospheric density, kg/m^3 ($slugs/ft^3$)
φ	roll attitude, deg
ω_n	undamped natural frequency, rad/sec

Subscripts:

d	Dutch roll mode
L	left
o	initial condition
R	right
rs	roll-spiral mode (lateral phugoid)
sp	short-period mode

A dot over a quantity represents the derivative of that quantity with respect to time.

VEHICLE DESCRIPTION

General

The M2-F2 was a single-place, wingless, research vehicle (figs. 1 and 2). The design was basically a blunt, 0.227 radian (13°) half cone with a flat upper surface and a boattailed afterbody. Two vertical fins were mounted high on the afterbody and equipped with trailing-edge rudders. The upper trailing edge of the afterbody was provided with two flaps, and the lower afterbody trailing edge was provided with a single-section

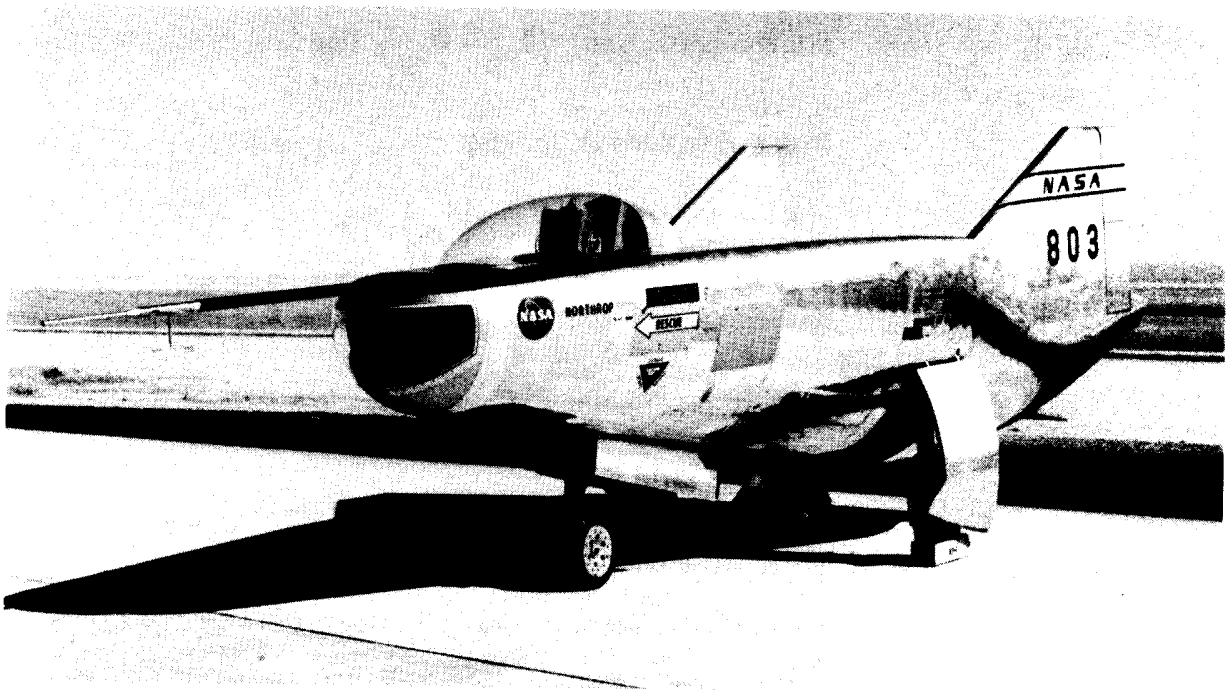

Figure 1. M2-F2.

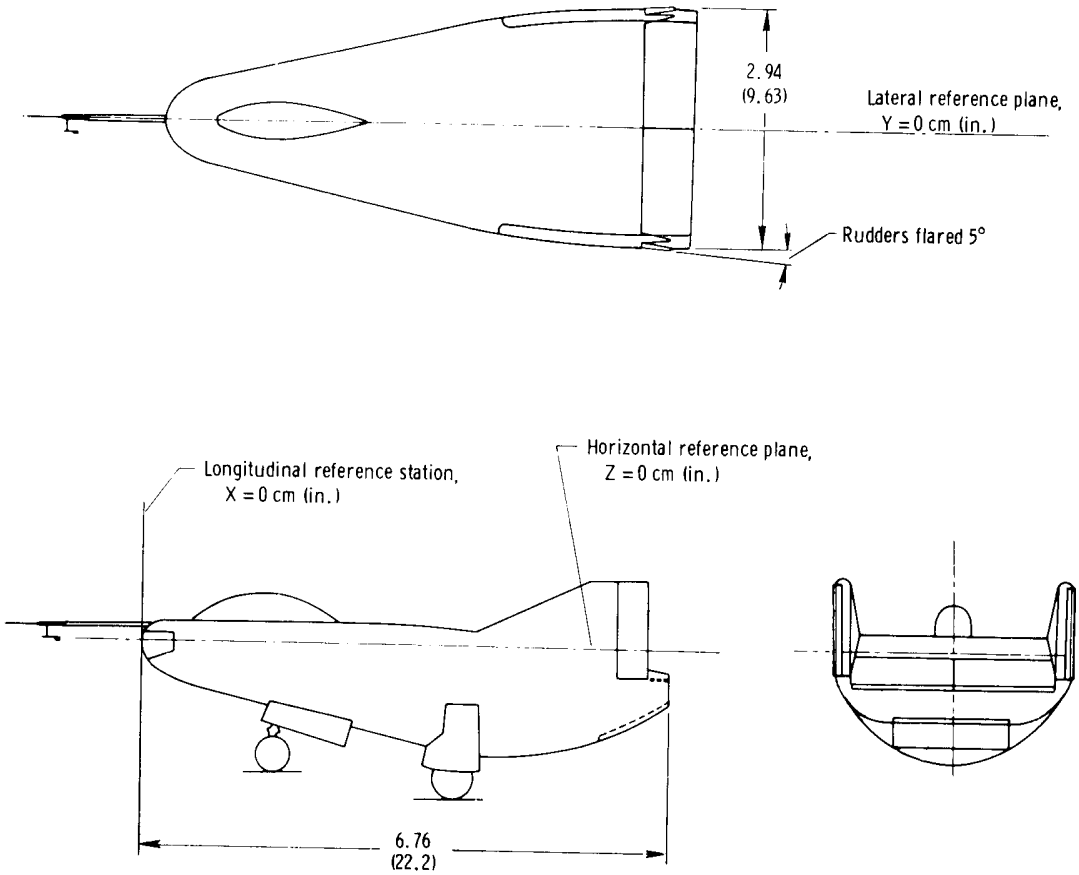

Figure 2. Three-view drawing of the M2-F2 vehicle. Dimensions in meters (feet) unless otherwise indicated.

flap (figs. 2 and 3). The structure incorporated a semimonocoque construction with

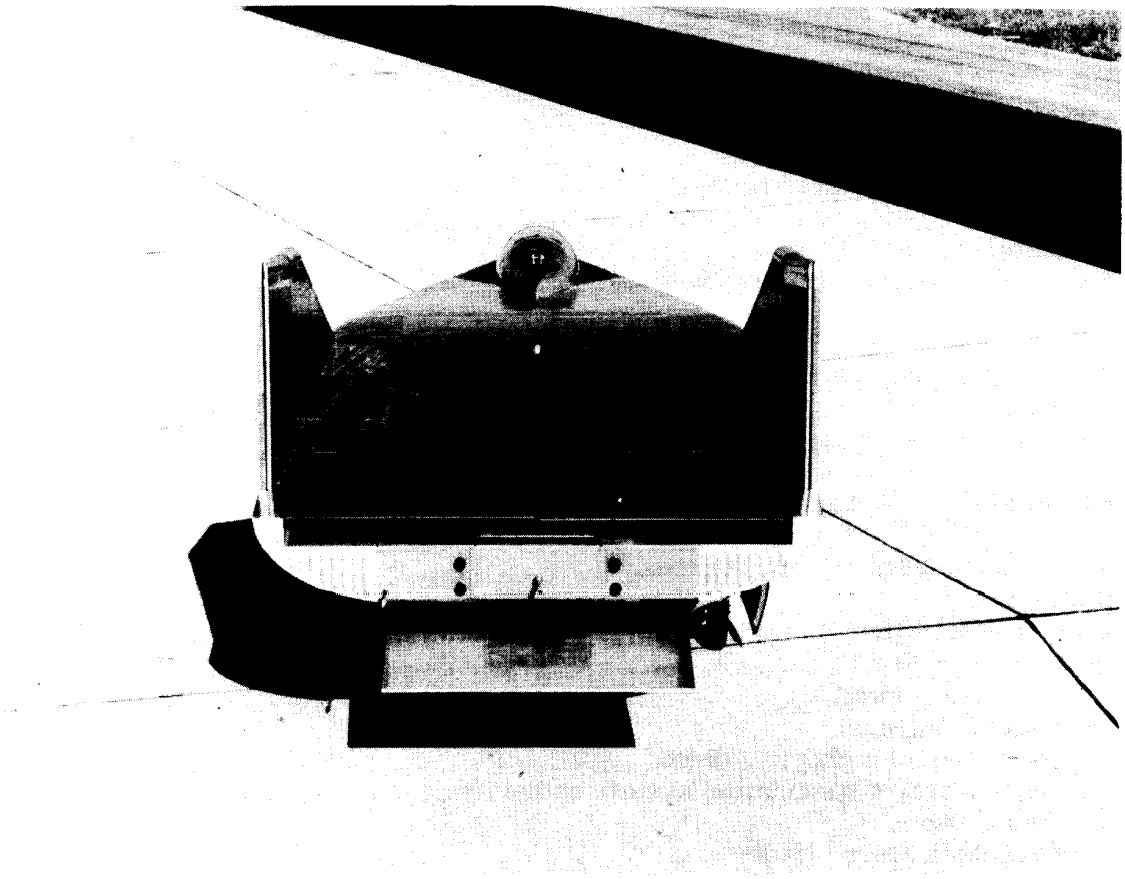

Figure 3. Rear view of the M2-F2.

two full-depth keels. The physical characteristics of the M2-F2 are listed in tables 1, 2, and 3.

Flight Control System

The flight control system of the M2-F2 was an irreversible, dual, hydraulic system. Conventional stick and rudder pedals were provided for roll, pitch, and yaw control, and artificial feel was provided about all axes. Cockpit control displacements and gradients and corresponding control surface travels are summarized in tables 1 and 2.

Coarse pitch trim was provided by positioning the upper flap by means of a trim wheel in the cockpit. For fine pitch trim, the pilot positioned the lower flap by means of a trim switch on the control stick.

Pitch control was provided through longitudinal displacement of the control stick which positioned the lower flap. Roll control was provided through lateral displacement of the control stick which differentially positioned the upper flaps. Yaw control was

TABLE 1. – PHYSICAL CHARACTERISTICS OF THE M2-F2 VEHICLE

Body –	
Planform area, meters^2 (feet^2):	
Actual	14.9 (160)
Reference, S	12.9 (139)
Longitudinal length, meters (feet):	
Actual	6.76 (22.2)
Reference	6.11 (20.0)
Span, without rudder flare, meters (feet):	
Actual	2.94 (9.63)
Reference, b	2.91 (9.54)
Aspect ratio, $\frac{b^2}{S}$, basic vehicle	0.655
Body-leading-edge sweep, degrees	77
Lower flap –	
Area, meters^2 (feet^2)	1.41 (15.23)
Span, meters (feet)	1.65 (5.42)
Chord, meters (feet)	0.86 (2.81)
Deflection, degrees:	
Pilot's control authority, down	5 to 30
Pitch stability augmentation system authority	±5
Upper flaps, two –	
Area, each, meters^2 (feet^2)	0.89 (9.57)
Span, each, meters (feet)	1.31 (4.28)
Chord, meters (feet)	0.68 (2.23)
Deflection, each flap, degrees:	
Pitch trim (symmetric travel), up	0 to 35
Pilot's aileron authority (asymmetric travel)	±5
Roll stability augmentation system authority (asymmetric travel)	±2 1/2
Vertical stabilizers, two –	
Area, each, meters^2 (feet^2)	1.50 (16.10)
Height, trailing edge, meters (feet)	1.16 (3.79)
Chord, meters (feet):	
Root	2.24 (7.36)
Tip	0.79 (2.58)
Leading-edge sweep, degrees	62.3
Rudders, two –	
Area, each, meters^2 (feet^2)	0.49 (5.27)
Span, each, meters (feet)	1.28 (4.20)
Chord, meters (feet)	0.38 (1.25)
Deflection, each (outward), degrees:	
Pilot's effective control authority	12
Yaw stability augmentation system authority	4.2

TABLE 2.– FLIGHT CONTROL SYSTEM OF THE M2-F2

Axis	Control	Maximum displacement, cm (in.)	Force gradient, N/cm (lb/in.)	Control surface	Surface rate limits, deg/sec
Pitch	Longitudinal stick	±12.70 (±5)	8.75 (5)	Lower flap	25
Roll	Lateral stick	±7.62 (±3)	5.83 (3.33)	Differential upper flap	30
Yaw	Rudder pedal	±7.62 (±3)	25.9 (14.8)	Rudders	22

TABLE 3.– WEIGHT AND LONGITUDINAL CENTER OF GRAVITY AND MOMENTS OF INERTIA AND VERTICAL AND TRANSVERSE CENTER OF GRAVITY FOR THE FIRST 16 M2-F2 FLIGHTS

Flight	W,		Center of gravity location						I_X,		I_Y,		I_Z,		I_{XZ},		ϵ, deg
			X,		Y,		Z,										
	kg	lb	cm	in.	cm	in.	cm	in.	kg-m^2	slug-ft^2	kg-m^2	slug-ft^2	kg-m^2	slug-ft^2	kg-m^2	slug-ft^2	
1	2687	5932	330.2	130.0	0	0	-35.3	-13.9	1296.2	956.3	7567.2	5583.0	8139.2	6005.0	-565.2	-417.0	-4.8
2	2687	5932	330.2	130.0	0	0	-35.3	-13.9	1296.2	956.3	7567.2	5583.0	8139.2	6005.0	-565.2	-417.0	-4.8
3	2689	5935	330.2	130.0	0	0	-35.3	-13.9	1296.2	956.3	7567.2	5583.0	8139.2	6005.0	-565.2	-417.0	-4.8
4	2692	5943	329.9	129.9	1.0	0.4	-35.3	-13.9	1297.9	957.6	7442.5	5491.0	8147.6	6011.2	-573.6	-423.2	-4.8
5	2692	5943	329.9	129.9	1.0	0.4	-35.3	-13.9	1297.9	957.6	7442.5	5491.0	8147.6	6011.2	-573.6	-423.2	-4.8
6	2688	5933	330.2	130.0	1.3	0.5	-35.3	-13.9	1296.8	956.8	7562.7	5579.7	8133.3	6000.7	-570.5	-420.9	-4.8
7	2692	5943	329.9	129.9	1.0	0.4	-35.3	-13.9	1299.0	958.4	7592.0	5601.3	8169.3	6027.2	-576.2	-425.1	-4.8
8	2661	5875	330.5	130.1	1.3	0.5	-35.3	-13.9	1296.7	956.7	7560.6	5578.1	8131.3	5999.2	-569.9	-420.5	-4.7
9	2702	5965	330.2	130.0	1.0	0.4	-35.3	-13.9	1299.0	958.4	7592.0	5601.3	8169.3	6027.2	-576.1	-425.1	-4.8
10	2702	5965	330.2	130.0	1.0	0.4	-35.3	-13.9	1299.0	958.4	7592.0	5601.3	8169.3	6027.2	-576.1	-425.1	-4.8
11	2697	5954	330.5	130.1	1.0	0.4	-35.1	-13.8	1299.3	958.6	7583.2	5594.8	8151.4	6014.0	-579.0	-427.2	-4.8
12	2697	5954	330.5	130.1	1.0	0.4	-35.1	-13.8	1299.3	958.6	7583.2	5594.8	8151.4	6014.0	-579.0	-427.2	-4.8
13	2697	5954	330.5	130.1	1.0	0.4	-35.1	-13.8	1299.3	958.6	7583.2	5594.8	8151.4	6014.0	-579.0	-427.2	-4.8
14	2697	5954	330.5	130.1	1.0	0.4	-35.1	-13.8	1299.3	958.6	7583.2	5594.8	8151.4	6014.0	-579.0	-427.2	-4.8
15	2737	6043	329.4	129.7	0	0	-37.4	-14.7	1444.9	1066.0	8502.8	6273.3	9079.1	6698.5	-812.4	-599.4	-6.0
16	2786	6150	328.9	129.5	0	0	-37.4	-14.7	1405.3	1036.8	8586.1	6334.7	9142.0	6744.9	-811.1	-598.4	-5.9

provided through displacement of the rudder pedals. The surfaces operated about a 5° flared condition as illustrated in figure 2. In response to a pedal input, one surface moved out as the other moved in, although the rudder could not move inboard farther than the faired or 0° deflection point.

Because of the high adverse yaw created by aileron deflection, the M2-F2 was equipped with an aileron-to-rudder interconnect; that is, a mechanical system which deflected the rudder by an amount proportional to the aileron deflection. The desired ratio of rudder-to-aileron setting was determined by the pilot and was controlled through a wheel in the cockpit. This feature enabled the pilot to make coordinated turns by using aileron inputs only. For these tests the interconnect ratio was set at a nominal value of approximately -0.5.

Stability Augmentation System

A rate-feedback stability augmentation system (SAS) was incorporated about all axes to provide angular rate damping. The SAS mode and gains were controlled by the pilot by means of cockpit switches. Roll and yaw channels with high pass filters provided the capability of canceling or washing out SAS control surface inputs when the angular rates approached a constant. Constant rate rolling and yawing motion was therefore not impeded by SAS control surface deflections.

Weight, Balance, and Mass Distribution

Precise M2-F2 weight and balance measurements were made whenever vehicle weight and mass distribution changed significantly. These measurements then became the reference condition used for the digital computer program in the update computation of mass distribution characteristics for various loading conditions. This program computed vehicle weight, three-coordinate center-of-gravity locations, moments of inertia, product of inertia, and inclination of the principal axis. Computations were made by compiling the weight and location of each item of structure, hardware, instrumentation, expendable material, ballast, and miscellaneous equipment in the vehicle with respect to the reference axes. It was also necessary to correct the program by introducing a bogie weight which brought the computed weight and longitudinal center-of-gravity location into agreement with the actual reference weight and balance measurements. Table 3 presents the computed weight, three-coordinate center-of-gravity positions, and moments of inertia of the M2-F2 used in this analysis.

Before the M2-F2 was completely outfitted for flight, it was decided to determine experimentally the yawing moment of inertia, the product of inertia, and the inclination of the principal axis at a lightweight condition as a check on the digital computer program. Table 4 compares the experimentally determined weight, inertias, and centers

TABLE 4.- COMPARISON OF EXPERIMENTAL AND COMPUTED WEIGHT AND MASS DISTRIBUTION CHARACTERISTICS OF THE M2-F2

Quantity	Experimental	Calculated
W, kg (lb)	1519 (4976)	1519 (4976)
I_Z, kg-m^2 (slug-ft^2)	8080 (5958)	8025 (5925)
I_{XZ}, kg-m^2 (slug-ft^2)	-638 (-471)	-569 (-420)
Inclination of principal axis, deg	-5.3	-4.8
Vertical center of gravity below reference, cm (in.)	30.8 (12.1)	37.6 (14.8)
Horizontal center of gravity, cm (in.)	341 (134.1)	341 (134.1)

of gravity with computed values. It should be noted that the bogie weight was generally approximately 2 percent of the weighed reference value and never exceeded 3 percent. On the basis of these results the digital program was used with a high degree of confidence.

FLIGHT TESTS

The M2-F2 was air-launched from a B-52 aircraft at approximately 13,730 meters (45,000 feet) altitude and a Mach number of 0.65. All flights were unpowered glide flights and were made under strict visual flight rule (VFR) conditions. All landings were on Rogers dry lakebed, which is approximately 700 meters (2280 feet) above mean sea level.

All maneuvers were performed at angles of attack between -2.3° and 13.8° and at Mach numbers from 0.41 to 0.64. They consisted of the conventional pulse-type maneuvers used for stability and control analysis and large angle-of-attack excursions used for performance, lift, and drag analysis. Both lateral-directional and longitudinal SAS-off pulse maneuvers were performed for specific identification of aerodynamic stability derivatives. SAS-on maneuvers, with controls not held fixed, were also performed for analysis of aerodynamic stability and control derivatives. For the analysis of any single M2-F2 flight response, the time interval was generally from 5 to 8 seconds. Short times were used primarily to maintain tolerable limits from relative steady-state conditions.

INSTRUMENTATION

Data were acquired by means of a pulse code modulation (PCM) system. No provisions were made for recording data onboard the vehicle. All data were sampled 200 times per second, conditioned, and transmitted to the ground station. On the ground the data were recorded on magnetic tape and processed, utilizing appropriate calibrations and corrections. Vehicle translational accelerations and angular rates were not corrected for instrument location because this factor was determined to be negligible. Airspeed and altitude were measured by using a NASA pitot static tube mounted on the nose boom (fig. 1). The static- and total-pressure orifices were, respectively, 1.704 meters (5.59 feet) and 1.905 meters (6.25 feet) ahead of the vehicle nose. The angle of attack and angle of sideslip were measured by free-floating vanes on the nose boom (fig. 1). The angle-of-attack vane was 1.20 meters (3.95 feet) ahead of the nose of the vehicle. The angle-of-sideslip vane was approximately the same distance from the nose of the vehicle, but oriented 90° to the axis of the angle-of-attack vane. Corrections for upwash and sidewash were applied to the angle-of-attack and angle-of-sideslip data. (See ref. 3.)

The basic accuracy of the PCM system was generally within 2 percent of full-scale deflection. The accuracies of the various parameters used in this report are presented in table 5.

TABLE 5.– ACCURACIES OF PERTINENT PARAMETERS

Parameter	Sensor accuracy, percent	Onboard PCM resolution, percent	Power supply accuracy, percent	Signal conditioning accuracy, percent	Calibration accuracy, percent	Root mean square, percent	Range parameter units	Root mean square parameter units
Angle of attack	0.5	0.25	0.5	0.5	0.6	1.08	40°	0.43°
Angle of sideslip	.5	.25	.5	.5	.6	1.08	20°	.22°
Pitch rate	1.0	.25	.5	.5	.6	1.38	40 deg/sec	.55 deg/sec
Roll rate	1.0	.25	.5	.5	.6	1.38	60 deg/sec	.83 deg/sec
Yaw rate	1.0	.25	.5	.5	.6	1.38	40 deg/sec	.55 deg/sec
Longitudinal acceleration	.5	.25	0	0	.6	0.82	1.0g	.0082g
Lateral acceleration	.5	.25	0	0	.6	.82	2.0g	.0164g
Normal acceleration	.5	.25	0	0	.6	.82	4.0g	.0328g
Roll attitude	1.0	.25	.5	.5	.6	1.38	180°	2.48°
Pitch attitude	1.0	.25	.5	.5	.6	1.38	90°	1.24°
Altitude (fine) scale	1.4	.25	.5	.1	.6	1.62	11,000 N/m^2 (230 lb/ft^2)	178.60 N/m^2 (3.73 lb/ft^2)
Airspeed scale	2.2	.25	.5	.1	.6	2.35	6700 N/m^2 (140 lb/ft^2)	157.5 N/m^2 (3.29 lb/ft^2)
Upper-flap positions	1.0	.25	.1	.1	.6	1.20	55°	.66°
Calculated average upper flap	---	----	---	---	---	1.69	55°	.93°
Upper-flap trim wheel position	1.5	.25	.1	.1	.6	1.64	35°	.58°
Calculated aileron	---	----	---	---	---	1.69	55°	.93°
Rudder positions	1.0	.25	.1	.1	.7	1.25	22°	.27°
Calculated average rudder	---	----	---	---	---	1.72	22°	.38°
Lower-flap position	1.0	.25	.1	.1	.6	1.20	35°	.42°

METHODS OF ANALYSIS

An analog-computer-matching analysis procedure was used in this study. This procedure is generally applicable to any aerodynamic vehicle, and particularly to motion which is separable into longitudinal or lateral-directional components with continuous control inputs. In the analog-matching technique, the equations of motion representing the mathematical model were programed on an analog computer. The computer was "forced" to solve the equations of motion based on the vehicle flight-recorded control surface inputs (forcing functions) as a function of time. Each analysis consisted of a maneuver at a specific time and time interval for a particular set of flight conditions. All flight-recorded variables of interest were stored in a digital computer and displayed to a human operator on a cathode ray tube (CRT). The computer was operated at a rate faster than real time so that the computer solutions and recorded flight time histories could be displayed on the CRT simultaneously as standing wave forms. By manually adjusting the aerodynamic stability and control derivatives of the computer-mechanized mathematical model, the operator attempted to match the computer-generated response with the measured vehicle flight response. This process of curve fitting, or difference minimization, allowed an experienced operator to make judgments and tradeoffs on the basis of phase and amplitude relationships and to manually adjust the derivatives accordingly. He could also disregard information which appeared to be incorrect. A match was considered to be achieved when a minimum difference was obtained simultaneously between all the flight-recorded and computed variables. More detailed information concerning the process of extracting aerodynamic stability derivatives from flight results is included in references 5 to 8.

The equations of motion used throughout this study were linearized, rigid-body equations referenced to vehicle body axes. These equations, which are developed in references 9 to 13, are presented in the appendix. The longitudinal calculations were generally based on two-degree-of-freedom equations with a provision for linear variations of dynamic pressure when conditions dictated. The longitudinal parameters matched were q, Θ, α, and a_n. Three-degree-of-freedom lateral-directional equations were used. Lateral-directional parameters matched were p, φ, β, r, and a_y. When longitudinal or lateral-directional, pulse-type, SAS-off maneuvers were performed, simplified approximate analyses were used to corroborate the results of the matching process. The simplified equations used in the computation of the approximate derivatives are also presented in the appendix.

RESULTS AND DISCUSSION

Longitudinal Static Stability and Control

The operational flight corridor of the M2-F2 is shown in figure 4 in terms of upper and lower limits of dynamic pressure. The data points indicate conditions for which longitudinal maneuvers were analyzed.

The least troublesome mode, in terms of derivative extraction, was the longitudinal short-period mode. The dampers-off, short-period-pulse, transient response maneuvers matched were determined to be essentially linear, thus validating the use of linearized equations in the analysis. A typical pulse-induced, longitudinal, short-period,

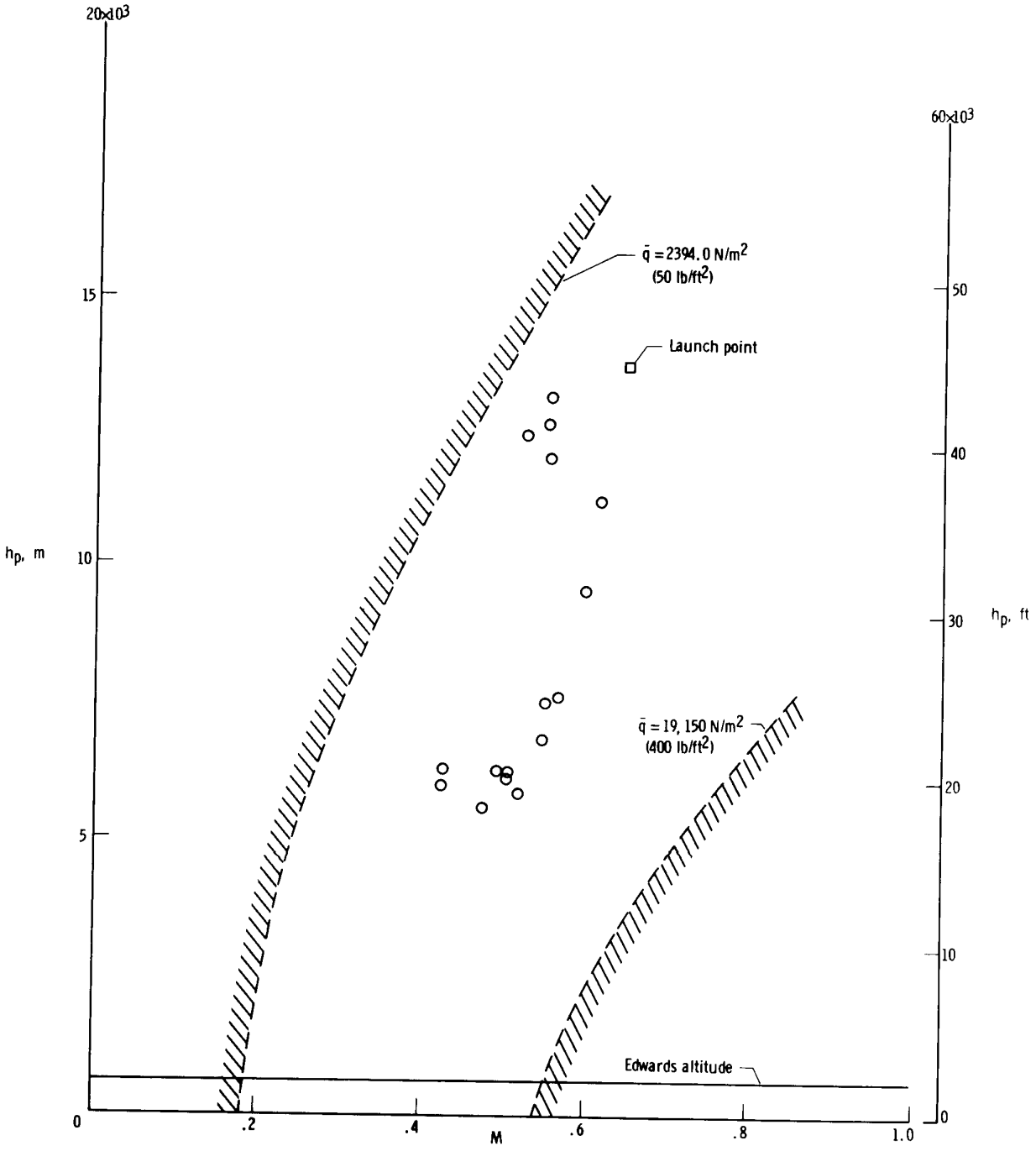

Figure 4. M2-F2 flight corridor, indicating conditions for which longitudinal maneuvers were analyzed.

dampers-off, flight transient response and the computer-generated, matched time history are presented for comparison in figure 5. This is considered to be a relatively good match.

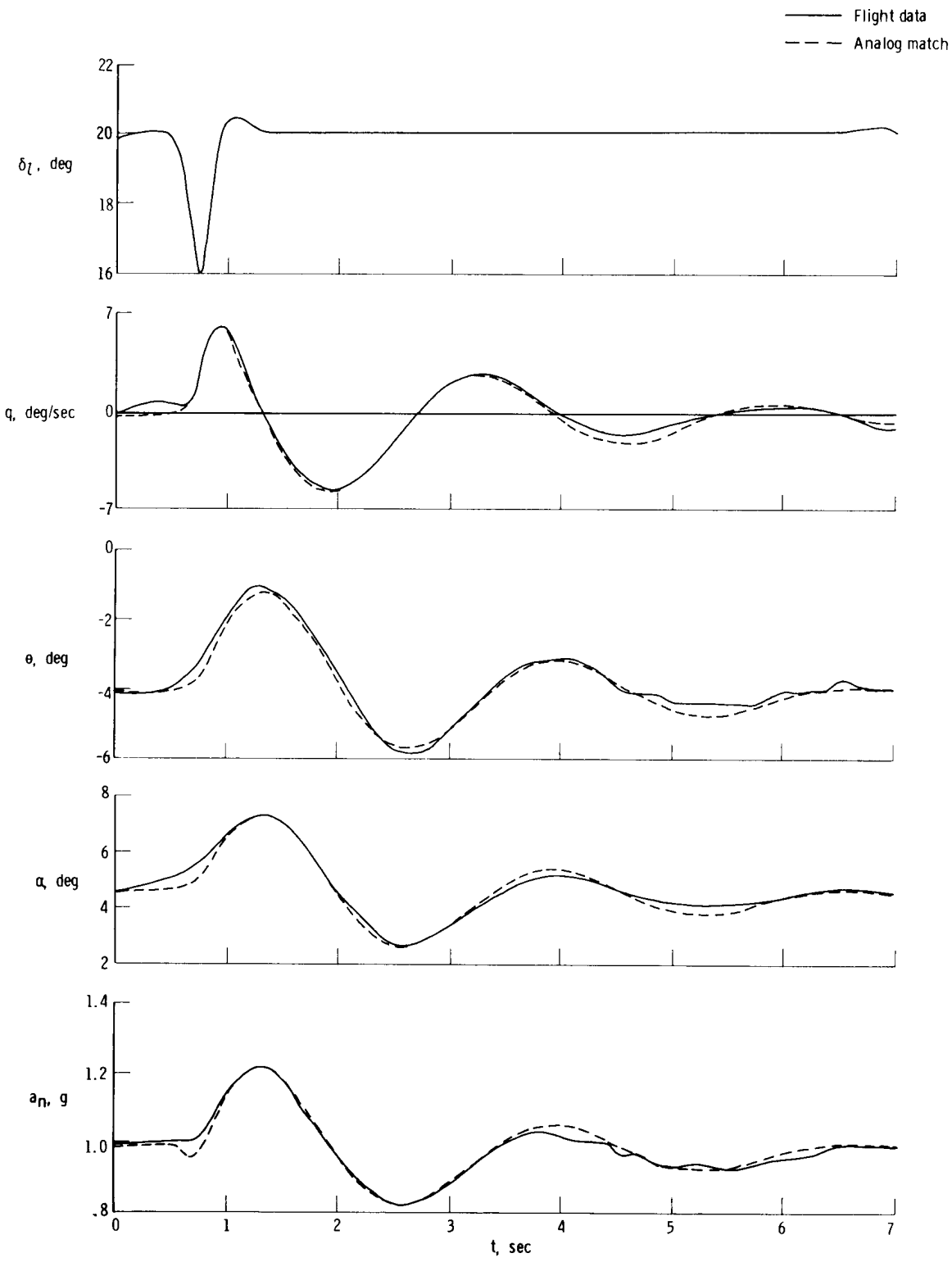

Figure 5. Flight-measured and analog-generated longitudinal short-period-mode time history of a pulse maneuver. SAS off; V = 182 m/sec (598 ft/sec); $\bar{q}$ = 5940 N/m^2 (124 lb/ft^2); M = 0.62.

Figure 6 is a semilogarithmic plot of the half-amplitude envelope of the flight-measured transient response of figure 5 (Δt is measured from the time where δ_l returns to its static position). The exponential decay in the response variable amplitude is typical of the response of linear systems. By using the approximate literal expressions

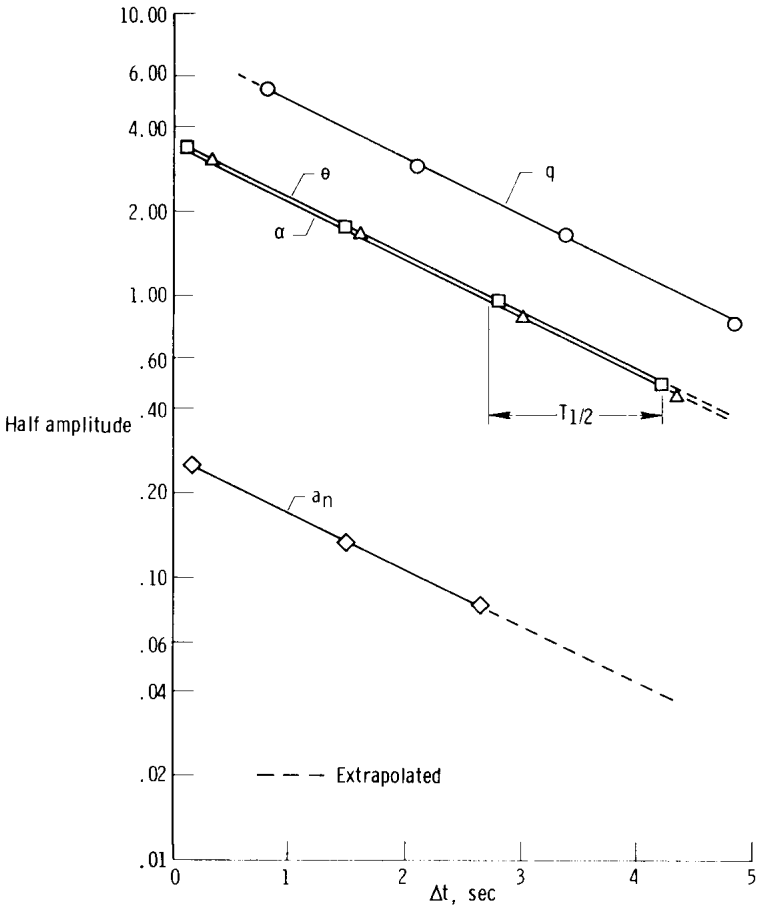

Figure 6. Amplitude versus time for the example flight-measured transient longitudinal response of figure 5. $T_{1/2}$ = 1.45 sec; P = 2.73 sec; $\zeta\omega_{n_{sp}}$ = 0.478 rad/sec; $\left|\frac{q}{\alpha}\right|$ = 2.26 per sec; $\omega_{n_{sp}}$ = 2.31 rad/sec.

presented in the Longitudinal Equations section of the appendix in conjunction with information from figure 6, the derivatives C_{m_α}, $C_{m_{\delta_l}}$, and $\left(C_{m_q} + C_{m_{\dot{\alpha}}}\right)$ were obtained for comparison with the matched derivatives. Table 6 compares the analog-matched and approximate derivative solutions for this flight condition. The agreement is

TABLE 6.– COMPARISON OF AERODYNAMIC DERIVATIVES DETERMINED BY ANALOG MATCHING AND BY SIMPLIFIED CALCULATIONS FOR ONE LONGITUDINAL PULSE

	C_{m_α}	$\left(C_{m_q} + C_{m_{\dot{\alpha}}}\right)$	$C_{m_{\delta_l}}$
Analog matching	-0.00169 per deg	-0.492 per rad	-0.00247 per deg
Simplified calculations	-.00146 per deg	-.666 per rad	-.00263 per deg

considered to be good, thus validating the use of the approximate derivative approach when pulse-type response data are available; however, the analog-matched derivatives are considered to be more correct because fewer approximations were used in obtaining them.

An example of a typical longitudinal flight maneuver time history with a random-appearing input and analog match is presented in figure 7. This is also considered to be a relatively good analog match.

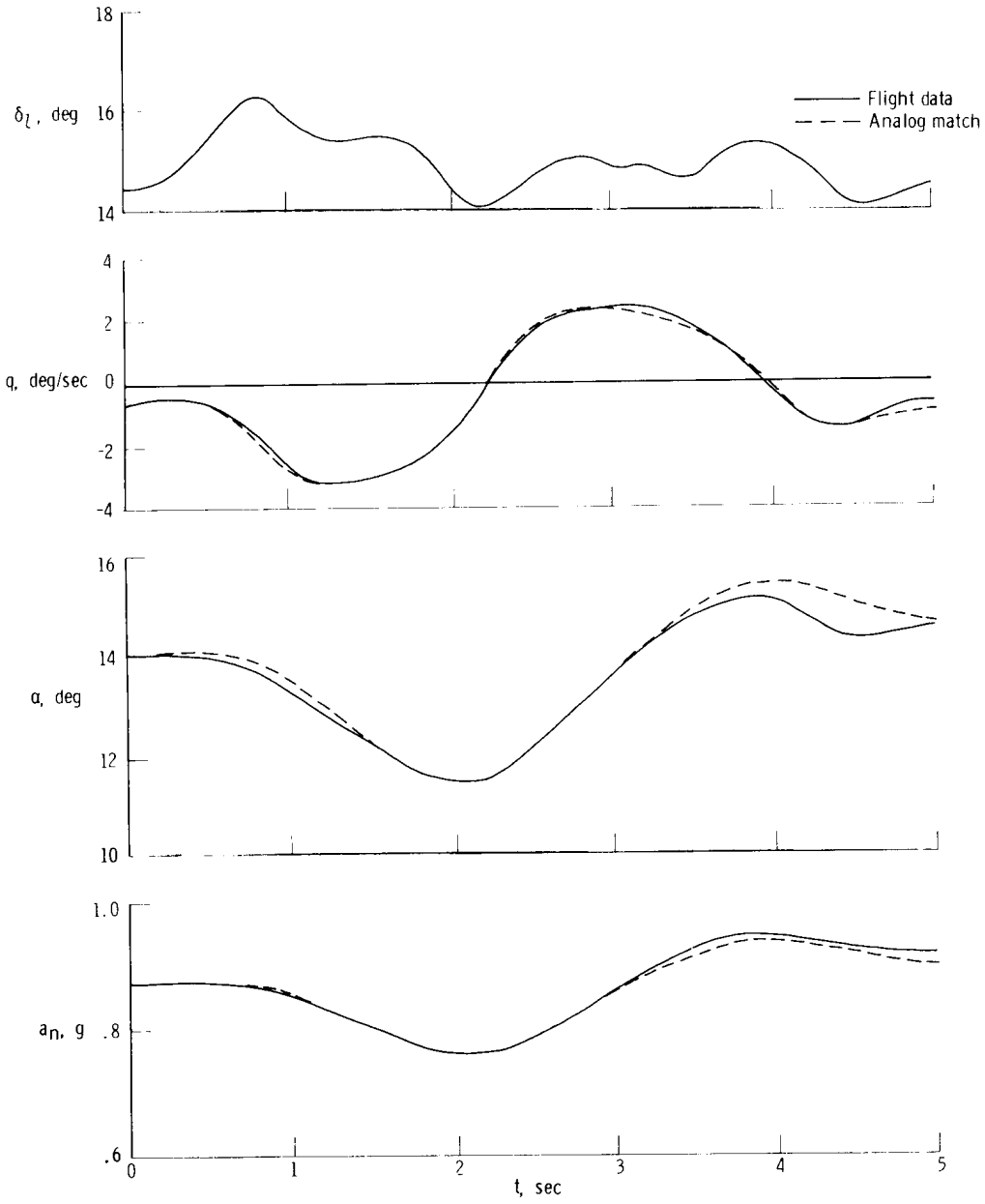

Figure 7. Flight-measured and analog-generated longitudinal random input time history. SAS on; V = 156 m/sec (512 ft/sec); $\bar{q}$ = 3480 N/m^2 (73 lb/ft^2); M = 0.53.

Table 7 summarizes the longitudinal flight data analyzed and the results obtained.

TABLE 7.– FLIGHT-MEASURED LONGITUDINAL AERODYNAMIC DERIVATIVES AND CALCULATED RESPONSE CHARACTERISTICS

$\bar{q}$,		α,	V,		h_p,		M	δ_u,	δ_l,	C_{m_α},	$(C_{m_q} + C_{m_{\dot{\alpha}}})$,	$C_{m_{\delta_l}}$,	C_{N_α},	ω_{sp},	$\zeta_{sp}\omega_{n_{sp}}$,
N/m^2	lb/ft^2	deg	m/sec	ft/sec	m	ft		deg	deg	per deg	per rad	per deg	per deg	rad/sec	rad/sec
5837	121.9	5.8	134.4	441	6,308	20,697	0.43	-11.3	19.4	-0.00121	-0.547	-0.00243	0.0232	2.089	0.518
5841	122.0	5.3	133.5	438	6,004	19,697	.42	-11.4	19.5	-.00146	-.657	-.00265	.0249	2.228	.606
7129	148.9	2.9	172.5	566	9,584	31,443	.60	-11.7	21.2	-.00182	-.475	-.00239	.0267	2.773	.464
7824	163.4	1.2	156.0	512	6,246	20,492	.49	-11.4	21.2	-.00129	-.479	-.00195	.0293	2.740	.613
8714	182.0	2.2	170.1	558	6,846	22,459	.54	-11.3	22.0	-.00145	-.507	-.00276	.0277	2.442	.591
5937	124.0	4.7	182.3	598	11,219	36,809	.62	-11.4	20.0	-.00169	-.492	-.00247	.0294	2.436	.389
4209	87.9	10.7	163.7	537	12,009	39,400	.56	-11.3	16.4	-.00151	-.446	-.00237	.0283	1.925	.281
8090	169.0	2.0	170.4	559	7,507	24,630	.55	-8.5	16.2	-.00174	-.400	-.00257	.0316	2.882	.507
8044	168.0	2.0	157.9	518	6,244	20,486	.50	-11.4	21.5	-.00164	-.654	-.00238	.0312	2.777	.747
9030	188.6	2.1	164.3	539	5,857	19,215	.52	-14.2	25.0	-.00162	-.579	-.00219	.0304	2.816	.484
8556	178.7	1.2	174.6	573	7,634	25,045	.56	-11.4	20.7	-.00157	-.415	-.00207	.0249	2.932	.734
3754	78.4	13.0	162.5	533	12,654	41,517	.55	-12.4	11.5	-.00098	-.400	-.00183	.0236	1.384	.204
7800	162.9	1.4	150.0	492	5,586	18,327	.47	-14.2	21.5	-.00129	-.560	-.00179	.0234	2.284	.568
8259	172.5	4.2	160.3	526	6,149	20,174	.51	-14.3	19.0	-.00132	-.400	-.00173	.0258	2.389	.465
3495	73.0	13.4	163.7	537	13,137	43,101	.56	-14.8	15.0	-.00125	-.475	-.00188	.0266	1.510	.216
3481	72.7	13.5	156.1	512	12,471	40,916	.53	-14.8	14.9	-.00108	-.400	-.00198	.0260	1.399	.199

Figure 8 is a comparison of M2-F2 wind-tunnel data and flight-determined static longitudinal derivatives. The wind-tunnel derivatives presented in this report were obtained from reference 14 and from unpublished data. All wind-tunnel data were adjusted to correspond to the flight vehicle center of gravity, which was approximately 54 percent of the reference vehicle length of 6.1 meters (20 feet). Full- and small-scale wind-tunnel data were measured about a moment reference center located at 55 percent of the reference length.

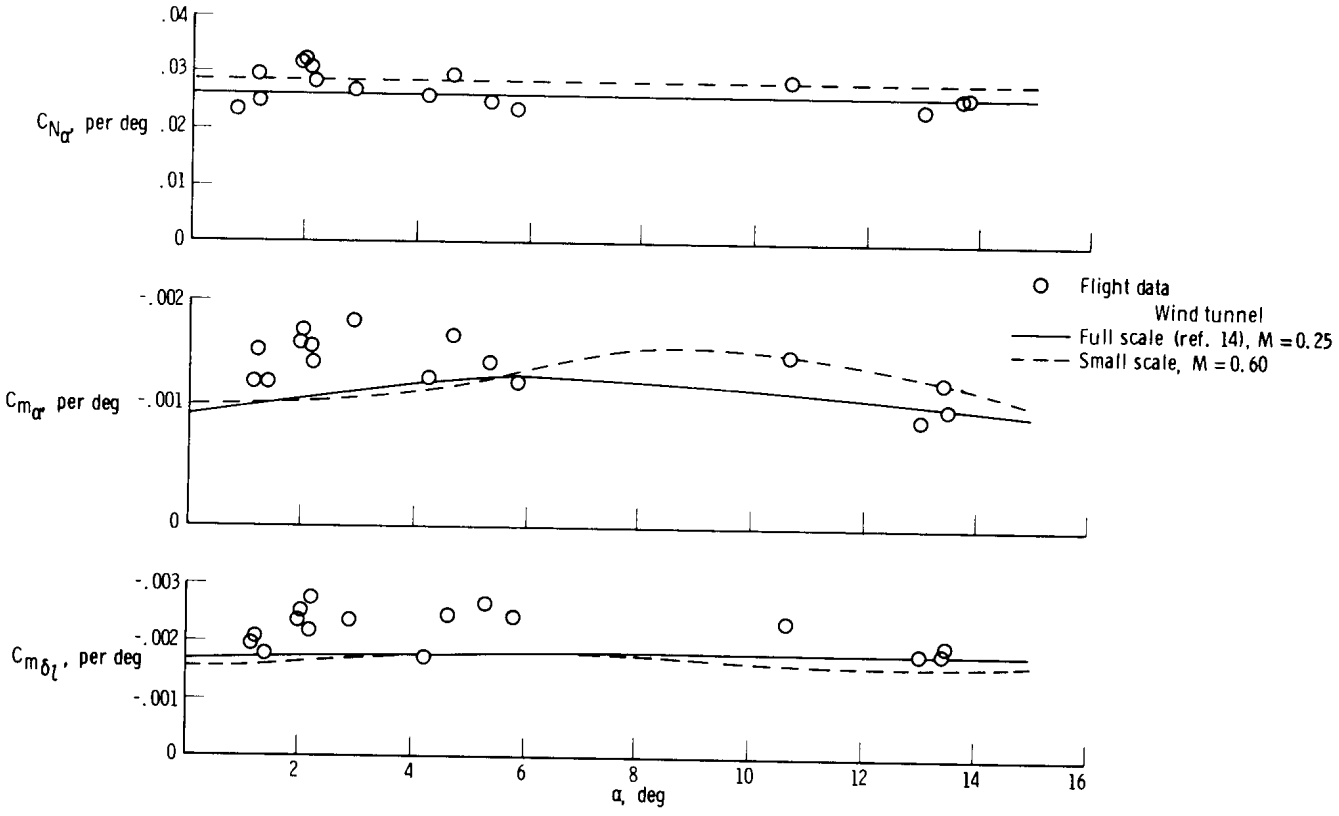

Figure 8. Comparison of M2-F2 wind-tunnel and flight-determined static longitudinal derivatives.

Values of the flight-determined derivative C_{m_α} at the low angles of attack were generally higher than predicted; at medium and higher angles of attack, the agreement was good. The flight-determined lower-flap effectiveness, $C_{m_{\delta_l}}$, was generally higher than comparable wind-tunnel data except at high angles of attack where agreement was good. The flight-determined normal-force-curve slope, C_{N_α}, was also generally in good agreement with tunnel predictions. The scatter band in the flight data of figure 8, although large in some of the data, would have been reduced if more data had been available and if better-conditioned flight maneuvers could have been performed. However, the results of this study are believed to be representative of a flight-test program of this type.

The longitudinal modal-response characteristics were calculated by using equations similar to the longitudinal equations in the appendix. The equations were solved by using a digital computer program in which the matched derivatives were the inputs. These data are presented in table 7.

Lateral-Directional Static Stability and Control

The operational flight corridor and related conditions for which lateral-directional flight maneuvers were analyzed are presented in figure 9. A typical example of a

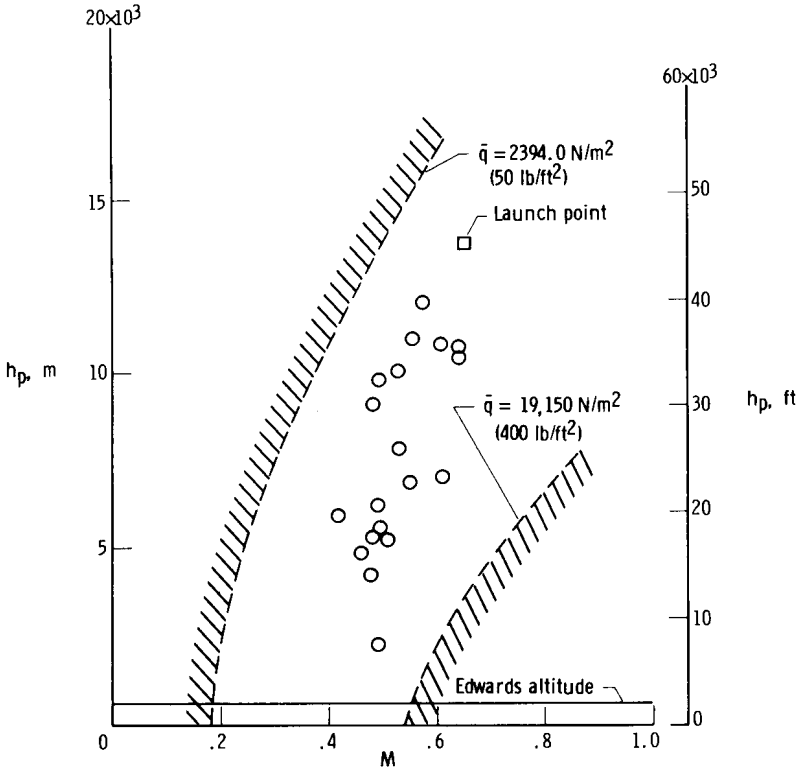

Figure 9. M2-F2 flight corridor indicating conditions for which lateral-directional maneuvers were analyzed.

flight-measured, lateral-directional maneuver with a continuous random input and its computer-matched time history is presented in figure 10. Figure 11 is a time history of a dampers-on, aileron-doublet pulse showing the flight response and computer match.

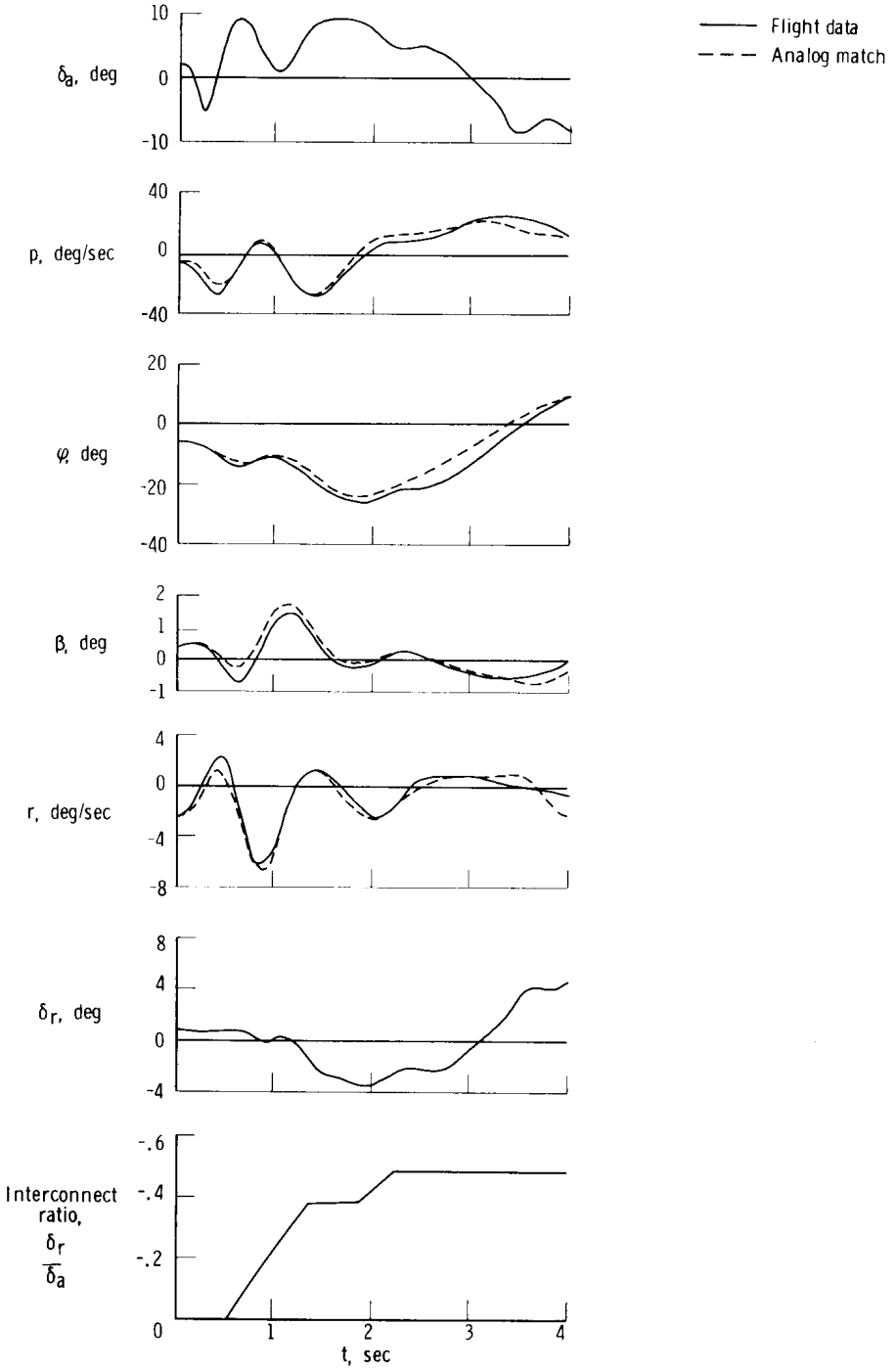

Figure 10. Flight-measured and analog-generated lateral-directional random input time history with varying aileron-to-rudder interconnect ratio. SAS on; $\alpha = 3.2^o$; $V = 196$ m/sec (642 ft/sec); $\bar{q} = 6910\ N/m^2$ (144.4 lb/ft^2); $M = 0.63$.

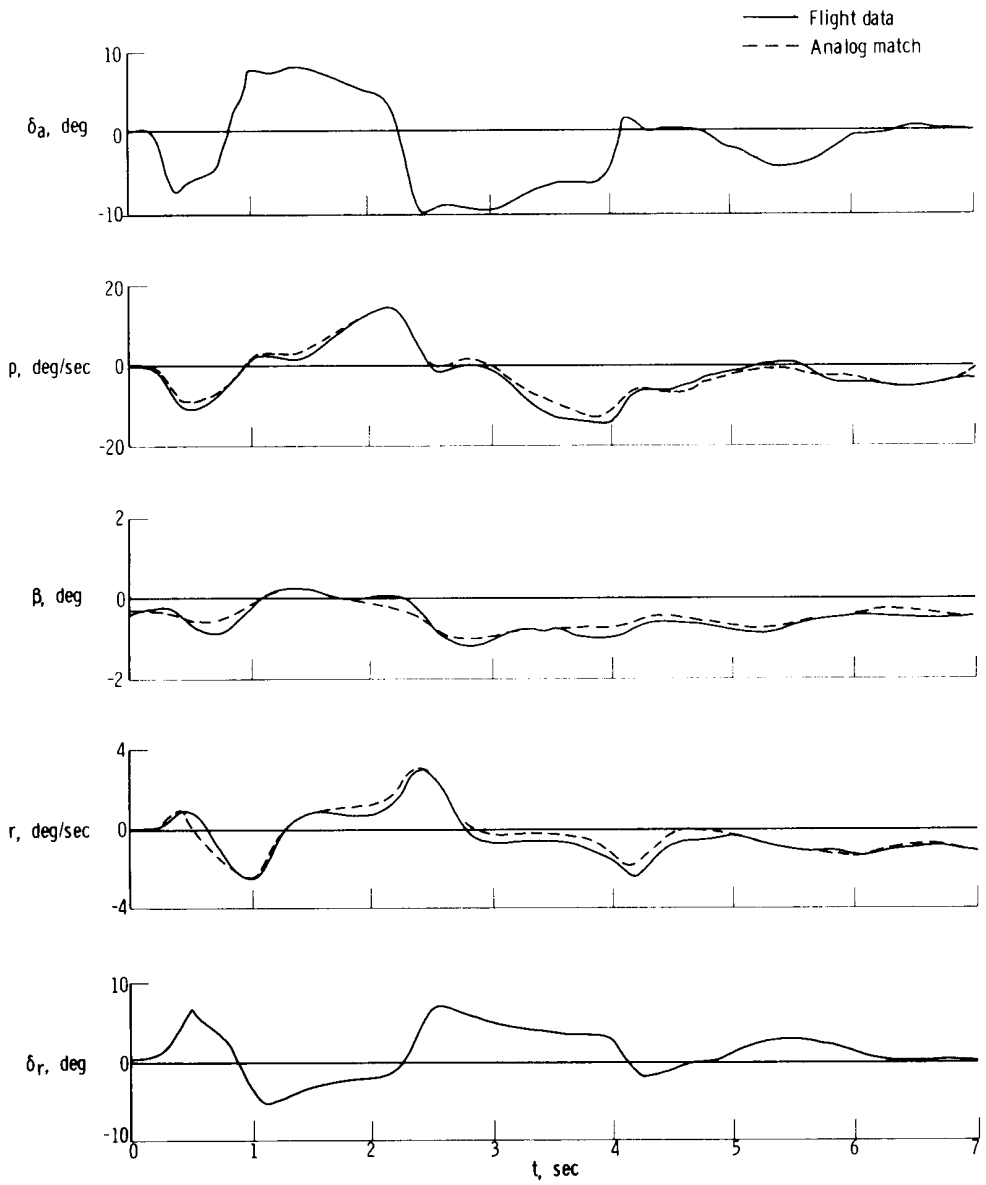

Figure 11. Flight-measured and analog-generated lateral-directional aileron-doublet input time history. SAS on; $\alpha = 3.1^{o}$; V = 164 m/sec (537 ft/sec); $\bar{q}$ = 7280 N/m^2 (152 lb/ft^2); M = 0.53.

Figure 12 presents a typical Dutch roll mode, dampers-off, transient response flight time history and the resulting computer match. Each of the computer-matched time histories of figures 10, 11, and 12 shows acceptable agreement with its respective flight response.

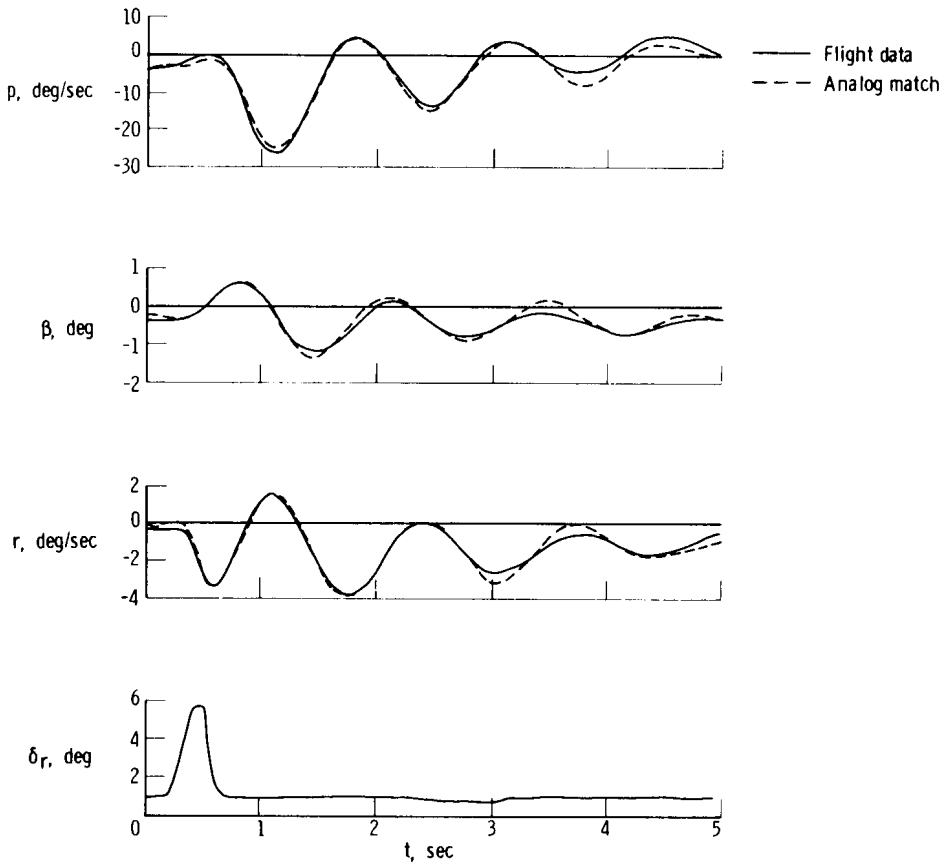

Figure 12. Flight-measured and analog-generated lateral-directional Dutch roll mode time history of a pulse maneuver. SAS off; α = 5.8°; V = 179 m/sec (587 ft/sec); q̄ = 6040 N/m² (126 lb/ft²); M = 0.61.

Figure 13 is a semilogarithmic plot of the half-amplitude envelope of the flight-measured transient response of figure 12 (Δt is measured from the time when δ_r returns to its static position). This plot was used in the simplified analysis and shows good linearity. The equations for the simplified approximations are contained in the Lateral-Directional Equations section of the appendix. The derivatives determined from the simplified approximations are compared in table 8 with the results from analog matching for the time history of figure 12. For this example, the directional-stability derivative, C_{n_β}, and the rudder-effectiveness derivative, $C_{n_{\delta_r}}$, determined from approximate equations show good agreement with the analog-matched values; however, the effective-dihedral derivative, C_{l_β}, is approximately 12 percent lower than the analog-matched value. It is interesting to note that the approximation for the effective-dihedral derivative is highly dependent on the measurement of the ratio of roll rate to sideslip angle. For the M2-F2 this ratio was generally between 3 and 15. The peak-to-peak amplitude of the sideslip angle measured in flight seldom exceeded 2°, and the effect of sidewash on the sideslip vane was not well defined; therefore, sideslip angle might be suspected as a source of possible error which could affect the C_{l_β} value determined.

A distinct advantage of the computer-matching technique is suggested in the foregoing discussion. If a particular parameter is needed but not required to accomplish a

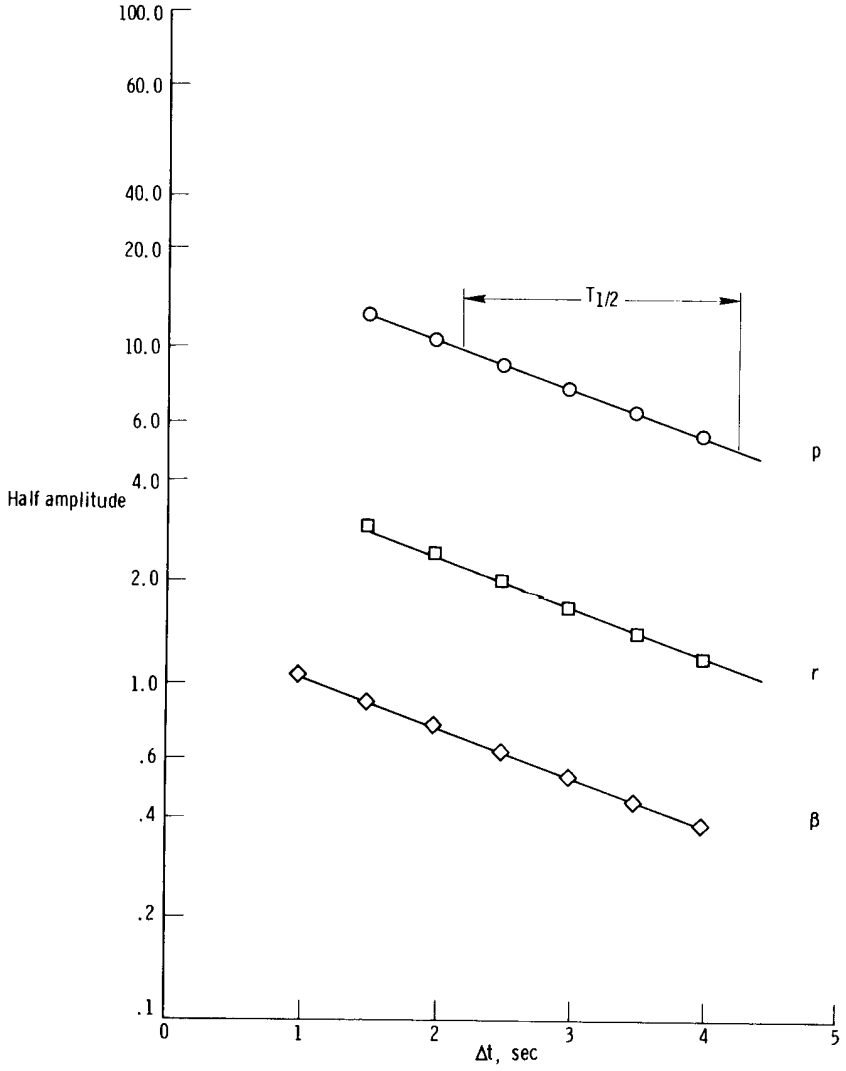

Figure 13. Amplitude versus time for the example flight-measured lateral-directional Dutch roll mode response of figure 12. $T_{1/2} = 2.04$ *sec;* $\zeta_d \omega n_d = 0.34$ *rad/sec;* $\omega n_d = 4.80$ *rad/sec;* $P = 1.31$ *sec;* $\left|\frac{p}{\beta}\right| = 14.2$; $\left|\frac{r}{\beta}\right| = 3.3$.

TABLE 8. – COMPARISON OF AERODYNAMIC DERIVATIVES DETERMINED BY ANALOG MATCHING AND BY SIMPLIFIED CALCULATIONS FOR A LATERAL-DIRECTIONAL PULSE

	C_{l_β}, per deg	C_{n_β}, per deg	$C_{n_{\delta_r}}$, per deg
Analog matching	-0.00796	0.00608	-0.00224
Simplified calculation	-.00700	.00628	-.00205

computer match, and that parameter is suspected of being in error or is possibly not available, the operator would adjust the credibility of that parameter accordingly in the matching process. That is, the operator would weight each parameter of the time history on the basis of the credibility of each and would make proper tradeoffs between the parameters in the time history which were known to be correct and those that were in error. The best compromise would be one that would result in the best set of derivatives for any particular case. It should be noted, however, that a best match does not necessarily represent the best set of derivatives.

Table 9 summarizes the lateral-directional responses for which analog matches were attempted and the results obtained. Figures 14(a) and 14(b) are plots of lateral-directional wind-tunnel and flight-determined static-stability and control derivatives. The wind-tunnel derivatives were obtained from reference 14 and unpublished data. The flight values of the dihedral derivative, C_{l_β}, the aileron-effectiveness derivative, $C_{l_{\delta_a}}$, and the rolling-moment-due-to-rudder-deflection derivative, $C_{l_{\delta_r}}$, are in good agreement with wind-tunnel results (fig. 14(a)). Flight values of the directional-stability derivative, C_{n_β}, the rudder-effectiveness derivative, $C_{n_{\delta_r}}$, and the yawing-moment-due-to-aileron-deflection derivative, $C_{n_{\delta_a}}$, are also in good agreement with wind-tunnel predictions (fig. 14(b)). It was not generally possible to detect differences in the aerodynamic derivatives over the Mach number range (0.42 to 0.64) of these tests, although the possibility that Mach effects were present should not be precluded.

The lateral-directional modal-response characteristics were calculated by using equations similar to those in the appendix. The equations were solved by using a digital computer program in which the matched derivatives were used as inputs. These data are presented in table 9. One interesting point indicated by this study was the relatively high ratio of bank-angle-to-sideslip-angle amplitude for the Dutch roll mode at low angles of attack due to the high value of the effective-dihedral derivative. Also of interest is the predicted existence of a coupled roll-spiral mode. Actual verification of this mode was difficult because of its strong dependency on the roll-damping derivative, C_{l_p}, and the cross-derivative, C_{n_p}. It should be noted that the response characteristics presented in table 9 are for the unaugmented (no dampers) vehicle and that the addition of rate damping would usually break this mode into the more common roll and spiral modes.

Longitudinal and Lateral-Directional Damping and Cross-Derivatives

Generally, the most difficult derivatives to predict are the cross-derivatives and the damping derivatives. Predicted values for the M2-F2 were obtained from a combination of theoretical estimates and unpublished wind-tunnel data. These predictions are believed to represent the best average values over the Mach and angle-of-attack range of interest. Also, because the analog-matching process is less sensitive to variations of the cross- and damping derivatives than to variations of any other derivatives, the damping derivatives are more difficult to obtain from flight responses. For example, in the analog-matching process it was possible to vary the predicted damping derivatives from 25 to 50 percent without seriously affecting a match. The cross-derivatives could have been changed from 50 to 200 percent without affecting a match.

TABLE 9.– FLIGHT-MEASURED LATERAL-DIRECTIONAL AERODYNAMIC DERIVATIVES AND CALCULATED RESPONSE CHARACTERISTICS

$\bar{q}$,		α,	V,		h_p,		M	δ_u,	δ_l,	C_{l_β},	C_{n_β},	$C_{l_{\delta_a}}$,	$C_{n_{\delta_a}}$,	$C_{l_{\delta_r}}$,	$C_{n_{\delta_r}}$,	C_{l_p},	C_{n_p},	C_{l_r},	C_{n_r},	ω_{n_d},	$\zeta_d\omega_{n_d}$,	$\left\lvert\frac{\varphi}{\beta}\right\rvert_d$	$\omega_{n_{rs}}$,	$\zeta_{rs}\omega_{n_{rs}}$,	$\left\lvert\frac{\varphi}{\beta}\right\rvert_{rs}$
N/m^2	lb/ft^2	deg	m/sec	ft/sec	m	ft		deg	deg	per deg	per deg	per deg	per deg	per deg	per deg	per rad	per rad	per rad	per rad	rad/sec	rad/sec		rad/sec	rad/sec	
8,750	182.7	1.3	156.4	513.0	5,603	18,381	0.49	-11.3	20.7	-0.00564	0.00218	0.000507	-0.000424	0.000377	-0.00146	[a](-0.3)	(0.2)	(0.4)	(-1.75)	3.635	0.749	6.617	0.466	0.0744	198.1
4,990	104.2	8.1	156.7	514.2	10,132	33,241	.53	-11.6	18.3	-.00986	.0092	.000643	-.000773	.000590	-.00154	-.3	(.2)	(.4)	(-1.75)	5.565	.360	2.893	.211	.1169	858.0
4,860	101.5	9.2	145.4	477.0	9,138	29,980	.48	-11.5	17.8	-.00767	.00554	.000926	-.000963	.000509	-.00194	-.239	(.2)	(.4)	(-1.75)	4.736	.350	2.983	.238	.1068	595.6
6,910	144.4	3.2	195.7	642.0	10,474	34,365	.63	-11.8	21.0	-.00862	.00422	.000710	-.000693	.000588	-.00159	(-.3)	(.2)	(.4)	(-1.75)	4.577	.454	5.041	.285	.0788	735.5
5,750	120.0	1.2	135.0	443.0	5,954	19,534	.42	-10.9	21.5	-.00537	.00440	.000429	-.000895	.000247	-.00156	-.31	.271	(.4)	-1.37	3.412	.445	4.790	.354	.1965	232.5
6,750	141.0	5.1	189.0	620.0	10,743	35,246	.64	-11.9	20.9	-.00725	.00466	.000744	-.000820	.000439	-.00186	(-.3)	(.2)	(.4)	(-1.75)	4.755	.451	3.851	.248	.0885	625.0
4,420	92.3	9.9	168.9	554.0	12,028	39,462	.57	-12.0	17.9	-.00964	.00607	.000514	-.00116	.000493	-.00155	(-.3)	(.2)	(.4)	(-1.75)	4.264	.303	2.522	.167	.0998	631.0
6,040	126.0	5.8	178.9	587.0	10,851	35,601	.61	-11.4	21.7	-.00796	.00608	.000525	-.000963	.000852	-.00224	(-.3)	.347	(.4)	-1.37	4.828	.276	3.575	.235	.1036	932.5
8,880	185.4	.6	171.9	564.0	6,897	22,623	.55	-11.3	22.1	-.00772	.00475	.000740	-.000704	.000440	-.00178	-.356	(.2)	(.4)	-1.90	4.190	.630	6.216	.403	.1296	329.7
9,630	201.2	-1.3	163.8	537.5	5,260	17,258	.51	-11.3	23.3	-.00549	.00279	.000609	-.000698	.000635	-.00182	(-.3)	(.2)	(.4)	(-1.75)	3.408	.681	8.120	.506	.1636	199.8
10,700	223.4	-1.6	191.1	627.0	7,080	23,229	.61	-11.1	22.7	-.00408	.00347	.000694	-.000828	.000489	-.00185	(-.3)	(.2)	(.4)	(-1.75)	3.622	.576	6.037	.371	.2274	276.2
4,830	100.9	9.5	163.3	535.8	11,014	36,138	.55	-11.2	17.2	-.00897	.00434	.00075	-.000950	.000550	-.00193	(-.3)	(.2)	(.4)	(-1.75)	4.852	.372	3.253	.230	.0869	679.8
4,640	97.0	12.7	147.8	485.0	9,848	32,310	.49	-12.4	12.2	-.01507	.00669	.000526	-.000930	.000600	-.00186	(-.3)	(.2)	(.4)	(-1.75)	6.441	.386	2.750	.217	.1041	1052.0
8,270	172.8	1.4	152.4	500.0	5,347	17,543	.48	-14.2	20.8	-.00702	.00389	.000638	-.000956	.000598	-.00196	-.232	.308	.45	(-1.75)	4.303	.633	5.174	.378	.1218	307.7
13,120	274.0	-2.3	162.2	532.0	2,264	7,429	.49	-14.4	22.8	-.00765	.00155	.000905	-.000706	.000349	-.00154	(-.3)	(.2)	(.4)	(-1.75)	3.645	1.051	12.760	.736	.0327	168.2
7,280	152.1	3.1	163.7	537.0	7,852	25,760	.53	-14.4	20.0	-.00878	.00428	.001057	-.000826	.000698	-.00179	(-.3)	.282	(.4)	(-1.75)	4.766	.534	4.740	.318	.0930	485.9
7,570	158.0	3.5	154.2	506.0	6,260	20,537	.49	-14.5	19.8	-.00668	.00239	.000747	-.000851	.000578	-.00197	(-.3)	(.2)	(.4)	(-1.75)	4.123	.612	4.978	.362	.0810	302.4
8,210	171.5	1.2	148.7	487.7	4,887	16,034	.46	-14.5	21.3	-.00895	.00336	.000758	-.000670	.000499	-.00136	(-.3)	(.2)	(.4)	(-1.75)	4.411	.642	6.184	.429	.1140	326.0
9,720	203.0	.7	155.4	510.0	4,233	13,887	.48	-14.5	21.7	-.00719	.00380	.000832	-.000970	.000797	-.00198	(-.3)	.174	(.4)	(-1.75)	4.541	.732	5.747	.423	.1400	297.2

[a]Values in parentheses represent predicted values (based on theoretical estimates and unpublished wind-tunnel data) used in matching and were not changed.

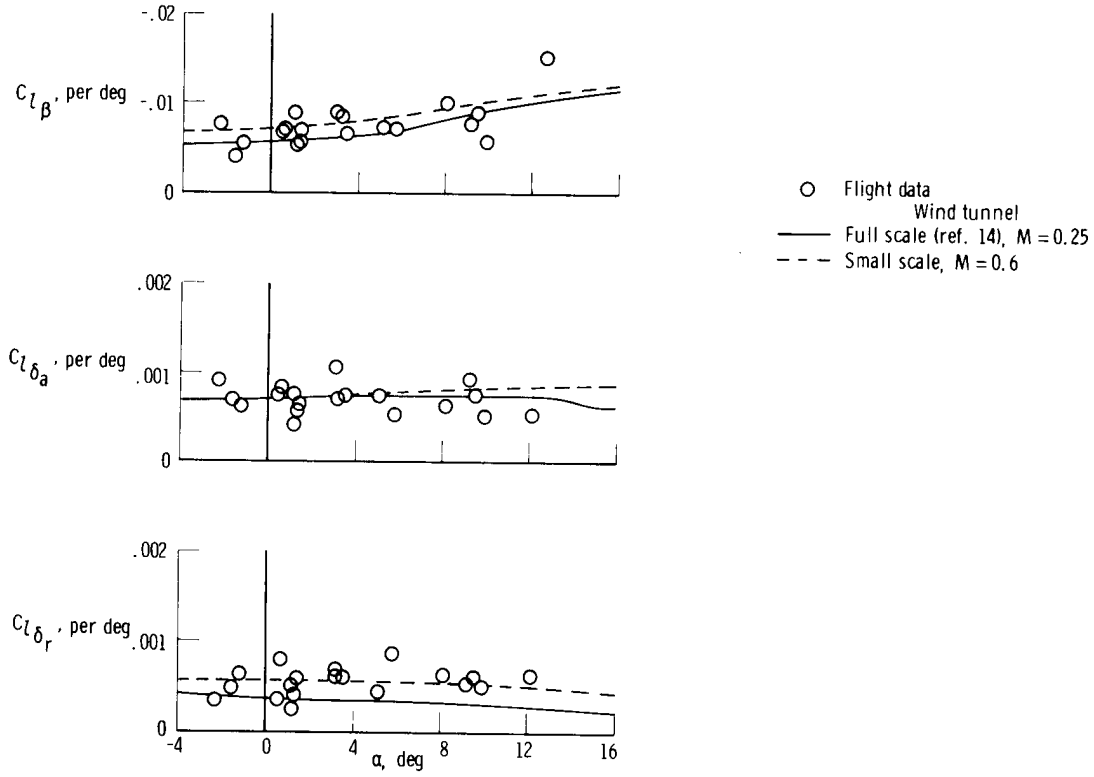

(a) Rolling-moment derivatives.

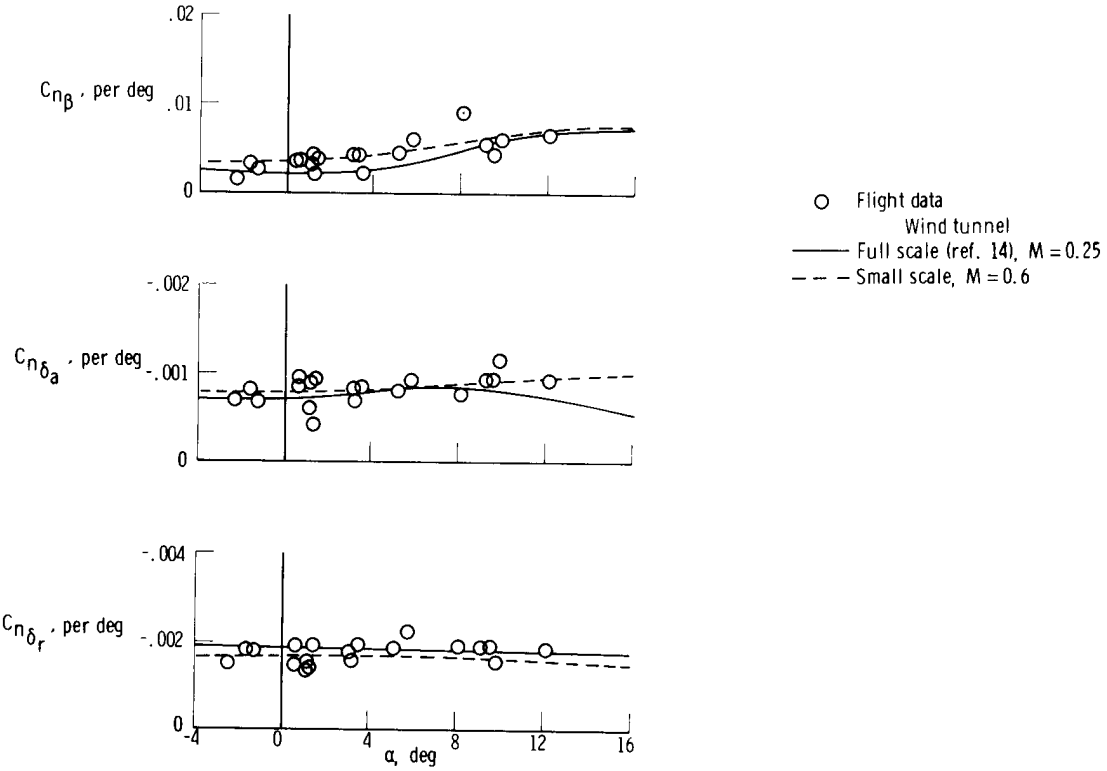

(b) Yawing-moment derivatives.

Figure 14. Comparison of M2-F2 flight and wind-tunnel lateral-directional rolling- and yawing-moment derivatives.

Values of the pitch-damping derivative, $\left(C_{m_q} + C_{m_{\dot{\alpha}}}\right)$, are shown in figure 15. The average flight-determined pitch-damping derivative was generally from 25 to 50 percent higher than predicted. This fact was corroborated by pilot comments concerning the

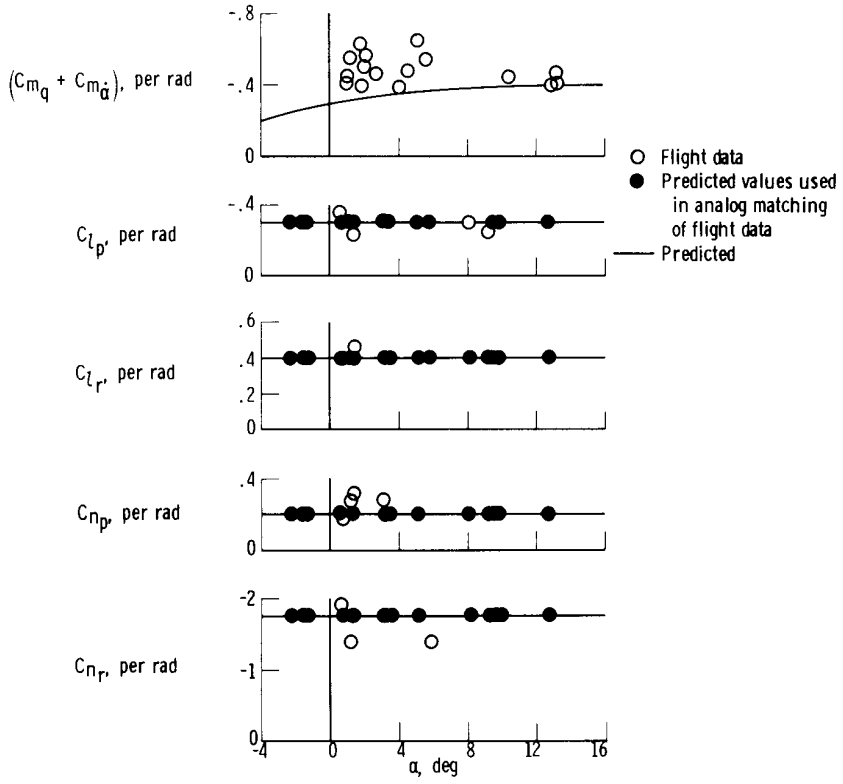

Figure 15. Comparison of M2-F2 flight-measured and predicted damping and cross-derivatives.

short-period-mode damping from flight pulses as compared with a flight simulation of the M2-F2 in which the predicted values were used.

The lateral-directional-damping derivatives and cross-derivatives are also shown in figure 15. All data used in the matching process are included, although in some instances the data were not changed from the predicted value because, as previously stated, moderate variations from these values had little effect on the individual match. In general, the roll-damping derivative, C_{l_p}, and the yaw-damping derivative, C_{n_r}, which were determined from flight data are in good agreement with predictions.

Side-Force Characteristics

The relative insensitivity of the transverse accelerometer used in the flight program precluded the determination of any reliable value of the side-force derivative, C_{Y_β}. As for the cross- and damping derivatives, the side-force derivative was difficult to obtain from the analog-matching process. As previously mentioned, the peak-to-peak amplitude of the sideslip angle seldom exceeded 2°. At a dynamic pressure of 14,400 N/m^2 (300 lb/ft^2), 1° of sideslip would produce approximately 0.1g transverse

acceleration. Figure 16 compares the wind-tunnel and flight-determined side-force derivatives. Only the data points which were considered valid are presented.

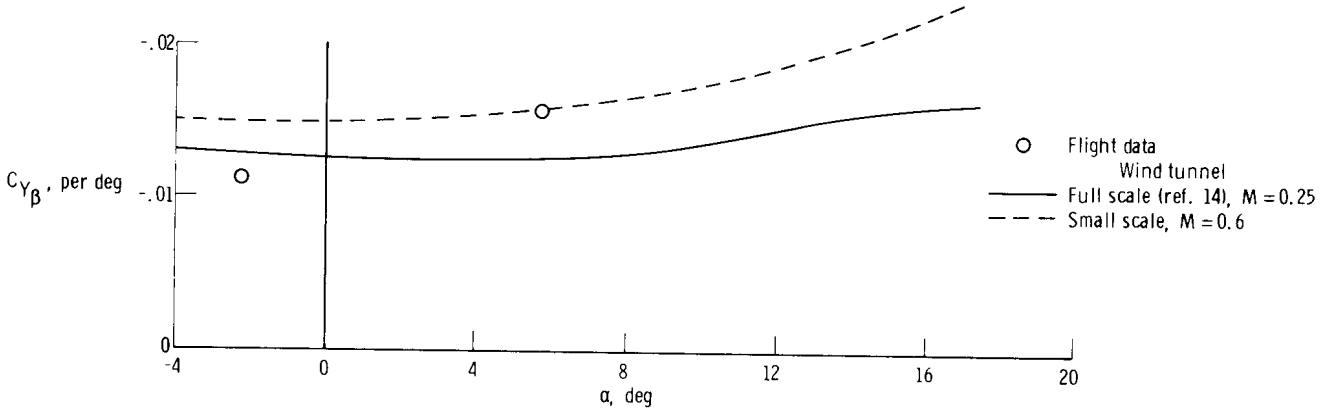

Figure 16. Comparison of side-force derivatives obtained from flight and wind-tunnel results.

CONCLUSIONS

Longitudinal and lateral-directional aerodynamic stability and control derivatives for the M2-F2 vehicle were extracted by using an analog computer program which matched the flight responses of the vehicle with corresponding computer responses. Analysis of the data from the first 16 glide flights revealed the following:

1. At low angles of attack the longitudinal static-stability derivative, C_{m_α}, was generally higher than predicted by wind-tunnel results. The lower-flap-effectiveness derivative, $C_{m_{\delta_l}}$, was also higher than predicted except at high angles of attack where agreement was good. The normal-force-curve slope, C_{N_α}, was in relatively good agreement with the predicted values.

2. The lateral-directional static-stability and control-effectiveness derivatives were in good agreement with the wind-tunnel-predicted values.

3. In general, the lateral-directional cross- and damping derivatives were in good agreement with the predicted values. However, the longitudinal pitch-damping derivative was 25 to 50 percent higher than predicted.

Flight Research Center,
National Aeronautics and Space Administration,
Edwards, Calif., July 21, 1971.

APPENDIX

EQUATIONS USED FOR DERIVATIVE DETERMINATION

Longitudinal Equations

Equations used in the mechanization of the analog-computer-matching process were as follows:

Normal-force equation

$$V(\dot{\alpha} - q) = Z_w w + Z_{\delta_l}\delta_l - (g \sin \Theta_o)\Theta$$

Pitching-moment equation

$$\dot{q} = M_w w + M_q q + M_{\dot{w}}\dot{w} + M_{\delta_l}\delta_l$$

The increment of normal acceleration as measured by a body-axes-oriented accelerometer is expressed as

$$\Delta a_n = \frac{V}{g}\left[\dot{\alpha} - q + g(\sin \Theta_o)\Theta\right]$$

Simplified approximations used in determining longitudinal static derivatives and damping derivatives are

$$\left(\omega_{n_{sp}}\right)^2 \approx Z_w M_q - V M_w$$

$$2\zeta_{sp}\omega_{n_{sp}} \approx -(Z_w + M_q + V M_{\dot{w}})$$

$$C_{N_\alpha} \approx \frac{W}{\bar{q}S}\frac{\Delta a_n}{\Delta \alpha}$$

$$C_{m_{\delta_l}} \approx \frac{I_X}{\bar{q}S\bar{c}}\left(\frac{\Delta \dot{q}}{\Delta \delta_l}\right)$$

Lateral-Directional Equations

Equations used in the mechanization of the analog-computer-matching process were as follows:

Rolling-moment equation

$$\dot{p} = \frac{I_{XZ}}{I_X}\dot{r} + L_\beta \beta + L_p p + L_r r + L_{\delta_a}\delta_a + L_{\delta_r}\delta_r$$

APPENDIX

Yawing-moment equation

$$\dot{r} = \frac{I_{XZ}}{I_Z}\dot{p} + N_\beta\beta + N_p p + N_r r + N_{\delta_a}\delta_a + N_{\delta_r}\delta_r$$

Side-force equation

$$\dot{\beta} = p\alpha_o - r + \left(\frac{g}{V}\right)\varphi + Y_\beta\beta + Y_{\delta_a}\delta_a + Y_{\delta_r}\delta_r$$

The increment of transverse acceleration as measured by a body-axes-oriented accelerometer is expressed as

$$a_y = \frac{V}{g}\left[\dot{\beta} + r - p\alpha_o - \left(\frac{g}{V}\right)\varphi\right]$$

Simplified approximations used in determining lateral-directional effective dihedral and directional-stability derivatives and the rudder-effectiveness derivative are

$$C_{l_\beta} \approx -\omega_{n_d}\left(\frac{I_X}{\bar{q}Sb}\right)\left(\left|\frac{p}{\beta}\right| + \frac{I_{XZ}}{I_X}\left|\frac{r}{\beta}\right|\right)$$

$$C_{n_\beta} \approx \omega_{n_d}\left(\frac{I_Z}{\bar{q}Sb}\right)\left(\left|\frac{r}{\beta}\right| + \frac{I_{XZ}}{I_Z}\left|\frac{p}{\beta}\right|\right)$$

$$C_{n_{\delta_r}} \approx \left(\frac{I_Z}{\bar{q}Sb}\right)\frac{1}{\Delta\delta_r}\left(\dot{r} - \frac{I_{XZ}}{I_Z}\dot{p}\right)$$

REFERENCES

1. Smith, Harriet J.: Evaluation of the Lateral-Directional Stability and Control Characteristics of the Lightweight M2-F1 Lifting Body at Low Speeds. NASA TN D-3022, 1965.

2. Holleman, Euclid C.: Stability and Control Characteristics of the M2-F2 Lifting Body Measured During 16 Glide Flights. NASA TM X-1593, 1968.

3. Pyle, Jon S.; and Swanson, Robert H.: Lift and Drag Characteristics of the M2-F2 Lifting Body During Subsonic Gliding Flight. NASA TM X-1431, 1967.

4. Mechtly, E. A.: The International System of Units - Physical Constants and Conversion Factors. NASA SP-7012, 1969.

5. Eckhart, Franklin F.: Analysis of Longitudinal Responses of Unstable Aircraft. Rep. No. BA-1610-F-1, Cornell Aeronautical Lab., Inc., Sept. 1964.

6. Rampy, John H.; and Berry, Donald T.: Determination of Stability Derivatives From Flight Test Data by Means of High Speed Repetitive Operation Analog Matching. FTC-TDR-64-8, Air Force Flight Test Center, May 1964.

7. Wolowicz, Chester H.; and Holleman, Euclid C.: Stability-Derivative Determination From Flight Data. AGARD Rep. 224, 1958.

8. Marchetti, Robert M.: Extraction of Aerodynamic Derivatives from Flight Data, Using an Analog Regression Technique. J. Aircraft, vol. 5, no. 1, Jan.-Feb. 1968, pp. 22-26.

9. Nelson, F. R.; Koerner, W.; and Trudel, R. E.: Dynamics of the Airframe. BuAer Rep. AE-61-4II, Sept. 1952.

10. Kempel, Robert W.: The Hypersonic Lateral-Directional Dynamics of Lifting Reentry Vehicles. FTC-TR-64-46, Air Force Flight Test Center, Aug. 1965.

11. Ashkenas, Irving L.; and McRuer, Duane T.: Approximate Airframe Transfer Functions and Application to Single Sensor Control Systems. Tech. Rep. 58-82 (ASTIA No. AD 151025), Wright Air Dev. Center, U. S. Air Force, June 1958.

12. Walker, Harold J.; and Wolowicz, Chester H.: Stability and Control Derivative Characteristics of the X-15 Airplane. NASA TM X-714, 1962.

13. Wolowicz, Chester H.: Considerations in the Determination of Stability and Control Derivatives and Dynamic Characteristics From Flight Data. AGARD Rep. 549 - Part 1, 1966.

14. Mort, Kenneth W.; and Gamse, Berl: Full-Scale Wind Tunnel Investigation of the Aerodynamic Characteristics of the M2-F2 Lifting-Body Flight Vehicle. NASA TM X-1588, 1968.